



RESEARCH

Open Access



Tau in cerebrospinal fluid induces neuronal hyperexcitability and alters hippocampal theta oscillations

Jessica Brown^{1,2}, Elena Camporesi³, Juan Lantero-Rodriguez³, Maria Olsson^{3,4}, Alice Wang¹, Blanca Medem¹, Henrik Zetterberg^{3,4,6,7,8,9,10}, Kaj Blennow^{3,4}, Thomas K. Karikari^{3,4,5} , Mark Wall¹ and Emily Hill^{1*} 

Abstract

Alzheimer's disease (AD) and other tauopathies are characterized by the aggregation of tau into soluble and insoluble forms (including tangles and neuropil threads). In humans, a fraction of both phosphorylated and non-phosphorylated N-terminal to mid-domain tau species, are secreted into cerebrospinal fluid (CSF). Some of these CSF tau species can be measured as diagnostic and prognostic biomarkers, starting from early stages of disease. While in animal models of AD pathology, soluble tau aggregates have been shown to disrupt neuronal function, it is unclear whether the tau species present in CSF will modulate neural activity. Here, we have developed and applied a novel approach to examine the electrophysiological effects of CSF from patients with a tau-positive biomarker profile. The method involves incubation of acutely-isolated wild-type mouse hippocampal brain slices with small volumes of diluted human CSF, followed by a suite of electrophysiological recording methods to evaluate their effects on neuronal function, from single cells through to the network level. Comparison of the toxicity profiles of the same CSF samples, with and without immuno-depletion for tau, has enabled a pioneering demonstration that CSF-tau potently modulates neuronal function. We demonstrate that CSF-tau mediates an increase in neuronal excitability in single cells. We then observed, at the network level, increased input–output responses and enhanced paired-pulse facilitation as well as an increase in long-term potentiation. Finally, we show that CSF-tau modifies the generation and maintenance of hippocampal theta oscillations, which have important roles in learning and memory and are known to be altered in AD patients. Together, we describe a novel method for screening human CSF-tau to understand functional effects on neuron and network activity, which could have far-reaching benefits in understanding tau pathology, thus allowing for the development of better targeted treatments for tauopathies in the future.

Keywords Tau, Electrophysiology, Cerebrospinal fluid, Tauopathy, Theta oscillations

*Correspondence:

Emily Hill

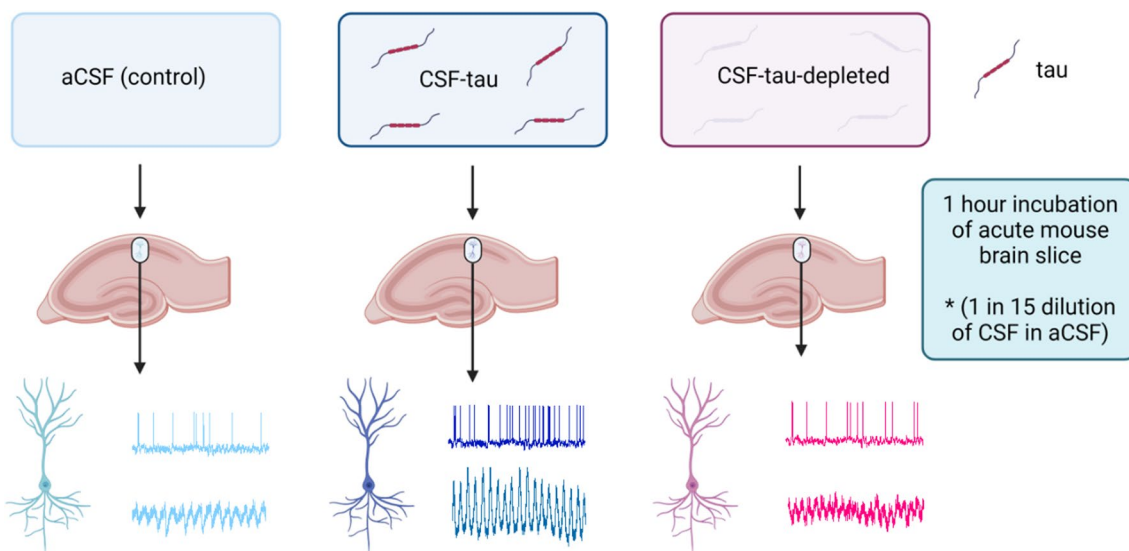
E.hill.4@warwick.ac.uk

Full list of author information is available at the end of the article



© The Author(s) 2023. **Open Access** This article is licensed under a Creative Commons Attribution 4.0 International License, which permits use, sharing, adaptation, distribution and reproduction in any medium or format, as long as you give appropriate credit to the original author(s) and the source, provide a link to the Creative Commons licence, and indicate if changes were made. The images or other third party material in this article are included in the article's Creative Commons licence, unless indicated otherwise in a credit line to the material. If material is not included in the article's Creative Commons licence and your intended use is not permitted by statutory regulation or exceeds the permitted use, you will need to obtain permission directly from the copyright holder. To view a copy of this licence, visit <http://creativecommons.org/licenses/by/4.0/>. The Creative Commons Public Domain Dedication waiver (<http://creativecommons.org/publicdomain/zero/1.0/>) applies to the data made available in this article, unless otherwise stated in a credit line to the data.

Graphical Abstract



Introduction

Tau plays a central role in the neuropathology of Alzheimer's disease (AD) and other tauopathies [69, 113]. Whilst insoluble high-molecular weight tau aggregates, including neurofibrillary tangles are more prominent in late phases of these diseases and can help to stage their pathological and clinical severity [21, 30, 95], the soluble forms of tau, including low-molecular weight aggregated and phosphorylated forms, are thought to be the most toxic species that modulate changes in neuronal function in the early stages of disease. In animal models of AD pathology, soluble tau aggregates have been shown to disrupt neuronal function, alter synaptic plasticity and impair cognitive function [20, 45, 81, 105, 108].

In AD, N-terminal to mid-domain tau fragments, both phosphorylated and non-phosphorylated variants, are released into the cerebrospinal fluid (CSF) early in disease progression, which has enabled the development of biomarkers for disease prognosis, diagnosis, and staging [19, 32, 57, 67, 110, 111]. While the presence of different tau forms in the CSF of AD patients is associated with neurofibrillary tangle pathology and cognitive decline [18, 29, 50, 64, 74, 90, 116], it is currently unclear whether the tau present in CSF is functionally active and could therefore modulate neural activity.

We have previously developed a technique using whole-cell patch-clamp recording to introduce structurally-defined soluble full-length recombinant tau aggregates into single neurons [60–62]. Using this approach,

we have been able to provide detailed characterisation of the pathological actions of soluble tau aggregates on single neuron electrophysiology, evaluate changes to synaptic transmission and plasticity, and demonstrate that the effects are specific to the aggregates as monomers had little or no effect [60, 61]. However, a limitation of using recombinantly produced tau is that it cannot represent the full range of endogenous tau forms present in the disease and delivery via a patch-pipette will only target a single neuron, thus, it is not possible to determine how these changes will modulate brain network function. To overcome these drawbacks, we have developed a new approach of incubating cortical slices in dilutions of patient CSF, which has allowed us to examine effects of clinically-derived tau species on single neurons and on cortical network activity (theta oscillations).

Active cortical networks support several rhythms (such as gamma and theta oscillations) that can be measured clinically including in individuals suspected to be affected by AD. Theta oscillations (4–7 Hz) represent the largest extracellular signal recorded in the mammalian brain [128] and are considered integral to hippocampal learning and memory processes [13, 15, 53]. Specifically, activity within the theta band reflects the temporal encoding of information and is thus associated with the consolidation and retrieval of episodic and spatial memory [85, 131]. Work on both rodent models of AD and human AD patients has shown that these rhythms and their coupling are disrupted as the pathology progresses [47, 66, 92, 93,

101, 112, 114]. In humans, changes in theta power have been widely reported during the performance of spatial navigation, working memory and recognition tasks [22, 26, 35, 42, 77, 106].

In this study, we have characterised the functional neurotoxic changes induced by tau-positive CSF samples, on neuronal function. We have used a suite of detailed electrophysiological measures; from single cells to network activity. We demonstrate that CSF-tau mediates an increase in neuronal excitability, alters synaptic transmission and plasticity and modifies the generation and maintenance of hippocampal theta oscillations. However, the same CSF samples, with tau removed by immuno-depletion, failed to produce these effects, indicating that tau is central to these neural changes.

Materials and methods

Collection, biomarker profiling and immuno-depletion of CSF

All CSF samples were obtained from patients by lumbar puncture from the L3/L4 or the L4/L5 inter-space in the morning, according to standardized procedure. Samples were collected in a propylene tube and centrifuged for 10 min at $1800\times g$ at $+4\text{ }^{\circ}\text{C}$. The supernatant was stored at $-80\text{ }^{\circ}\text{C}$ prior to use. The CSF samples used in this study were the remainder following clinical routine analyses, from multiple de-identified patients, pooled together in a procedure approved by the Ethics Committee at the University of Gothenburg (#EPN 140811). The collection and use of CSF samples were in accordance with the Swedish law of biobank in healthcare (2002:297).

The biomarker profile for the pool, including A β 42, A β 40, total tau (t-tau) and phosphorylated tau at threonine 181 (p-tau181), was measured with the fully automated Lumipulse (Fujirebio) platform following published protocols [51]. The CSF pool was then divided into two equal aliquots. To remove tau protein, aliquot 1 was immuno-depleted using immunoprecipitation (IP) following a previously established protocol [79] combining three antibodies to thoroughly cover across the full-length tau-441 sequence. Four μg of Tau12 (N-terminal [epitope=amino acids 6–18], BioLegend), HT7 (mid-region [epitope=amino acids 159–163], ThermoFisher), and TauAB (C-terminal [epitope=amino acids 425–441], kindly provided by MedImmune) were independently conjugated with 50 μL of M-280 Dynabeads (sheep anti-mouse IgG, Invitrogen) following manufacturer's recommendations. Beads were then mixed and added to aliquot 1. Incubation was performed overnight at $4\text{ }^{\circ}\text{C}$ on a rolling station to allow mixing of the beads with the sample and to avoid the beads forming aggregated deposits. The next morning, the beads were removed from the mixture by standing the tube against a magnet. The supernatant

was carefully pipetted out to obtain the CSF-tau-depleted fraction. Aliquot 2 underwent the same free-thaw cycle as the CSF-tau-depleted but was not immuno-depleted. Both samples were stored at $-80\text{ }^{\circ}\text{C}$ prior to use. To verify the removal of tau after the immuno-depletion, we used different assays that cover various regions of tau. The t-tau assay from Quanterix, p-tau181 [75] and p-tau231 [8] in house assays were used for tau measurements in both the CSF-depleted and the non-depleted aliquots on a Simoa HD-X instrument (Quanterix, Billerica, MA, USA) following methods originally described in the cited publications. To further validate the removal of tau, the CSF-depleted sample was also tested using the mid-region targeting Lumipulse p-tau-181 assay (Fujirebio) [51]. To confirm that the immuno-depletion process did not have effects (other than the removal of tau) that could contribute to observed changes, an aliquot of the full CSF pool underwent the same immuno-depletion process with a bead cocktail conjugated with anti-mouse IgG (GE healthcare) and neurogranin (H-6, Santa Cruz Biotechnology) antibodies, providing a 'mock-depletion' control. As a further control, we tested an individual control CSF sample from a 62-year-old female patient who was triple negative for amyloid pathology (A β 42), tau phosphorylation (p-tau181) and neurodegenerative (t-tau) as measured using the Lumipulse CSF assays. The effects of this control sample on neuronal function were compared to changes observed with the full CSF sample and the control artificial (a)CSF (Additional file 1: Fig. S1).

CSF collection and processing were performed at the University of Gothenburg, Sweden, with local ethical approval, and the samples sent to the University of Warwick, UK, where all experiments were done as approved by the local Human Tissue Authority and Biomedical & Scientific Research Ethics Committees.

Preparation of mouse brain slices

All animal care and experimental procedures were reviewed and approved by the institutional animal welfare and ethical review body (AWERB) at the University of Warwick. Animals were kept in standard housing with littermates, provided with food and water ad libitum and maintained on a 12:12 (light–dark) cycle. C57BL/6 mice (3–4-week-old; male and female) were killed by cervical dislocation and decapitated in accordance with the United Kingdom Animals (Scientific Procedures) Act (1986). The brain was rapidly removed, and acute parasagittal or horizontal brain slices (350–400 μm) were cut with a Microm HM 650 V microslicer in cold ($2\text{--}4\text{ }^{\circ}\text{C}$) high Mg^{2+} , low Ca^{2+} artificial CSF (aCSF), composed of the following: 127 mM NaCl, 1.9 mM KCl, 8 mM MgCl_2 , 0.5 mM CaCl_2 , 1.2 mM KH_2PO_4 , 26 mM NaHCO_3 , and

10 mM D-glucose (pH 7.4 when bubbled with 95% O₂ and 5% CO₂, 300 mOsm). Slices were stored at 34 °C in standard aCSF (1 mM Mg²⁺ and 2 mM Ca²⁺) for between 1 and 8 h.

Incubation of acute brain slices with CSF samples

After at least 1 h of recovery, slices were either incubated in aCSF (control) or in varying dilutions (1:15, 1:30, 1:100 in aCSF) of CSF-tau or CSF-tau-depleted (immunodepleted for tau) for 1 h, in bespoke incubation chambers at room temperature. The incubation chambers consisted of small, raised grids (to allow perfusion of slices from above and below) placed in the wells of a twenty-four well plate (Falcon) which were bubbled with 95% O₂, 5% CO₂ using microloaders (Eppendorf). Slices were placed into the incubation chambers one at a time (minimum volume 1.5 ml to cover raised grid). This pre-incubation protocol is an efficient method of exposing acute mouse brain slices to small volumes of diluted human CSF. The CSF sample volumes in this study and proposed for future studies (at the individual patient level) will not allow for perfusion of the diluted CSF through the recording rig (requiring at least 30–40 ml of solution). Therefore, following incubation individual slices were placed on the recording rig and perfused with regular aCSF throughout the recording period, so the CSF-tau was only present for the 1-h incubation. In further control experiments, slices were incubated in either CSF-mock-depleted (immunodepletion control using a combination of anti-mouse IgG and neurogranin antibodies) or CSF from a control patient (negative for amyloid, tau, and neurodegeneration) to further validate our findings (Additional file 1: Figs. S1 and S3).

Whole cell patch clamp recording from single hippocampal CA1 pyramidal neurons

A slice was transferred to the recording chamber, submerged, and perfused (2–3 ml/min) with aCSF at 30 °C. Slices were visualised using IR-DIC optics with an Olympus BX151W microscope (Scientifica) and a CCD camera (Hitachi). Whole-cell current-clamp recordings were made from pyramidal cells in area CA1 of the hippocampus using patch pipettes (5–10 MΩ) manufactured from thick-walled glass (Harvard Apparatus). Pyramidal cells were identified by their position in the slice, morphology (from fluorescence imaging) and characteristics of the standard step current–voltage relationship. Voltage recordings were made using an Axon Multiclamp 700B amplifier (Molecular Devices) and digitised at 20 kHz. Data acquisition and analysis were performed using pClamp 10 (Molecular Devices). Recordings from neurons that had a resting membrane potential of between – 55 and – 75 mV at whole-cell breakthrough were

accepted for analysis. The bridge balance was monitored throughout the experiments and any recordings where it changed by > 20% were discarded.

Stimulation protocols

To extract the electrophysiological properties of recorded neurons, both step, ramp and more naturalistic, fluctuating currents were injected.

Standard IV protocol

The standard current–voltage relationship was constructed by injecting standard (step) currents from – 200 pA incrementing by either 50 or 100 pA (1 s duration) until a regular firing pattern was induced. A plot of step current against voltage response around the resting potential was used to measure the input resistance (from the gradient of the fitted line).

Rheobase ramp protocol

To evaluate the rheobase (the minimum current required to elicit an action potential (AP)) a current ramp was injected into neurons. From the baseline, a 100 ms duration ramp to – 100 pA was followed by a 900 ms duration ramp at 0.33 pA/ms up to 200 pA, then a step back down to baseline (zero current).

Dynamic IV protocol

The dynamic I–V curve, defined by the average transmembrane current as a function of voltage during naturalistic activity, can be used to efficiently parameterize neurons and generate reduced neural models that accurately mimic the cellular response. The method has been previously described [10, 11, 58], for the dynamic-IV computational code, see [58]. Briefly, a current waveform, designed to provoke naturalistic fluctuating voltages, was constructed using the summed numerical output of two Ornstein–Uhlenbeck processes [125] with time constants $\tau_{fast}=3$ ms and $\tau_{slow}=10$ ms. This current waveform, which mimics the stochastic actions of AMPA and GABA-receptor channel activation, is injected into cells and the resulting voltage recorded (a fluctuating, naturalistic trace). The voltage trace was used to measure the frequency of action potential firing and to construct a dynamic I–V curve. The firing rate was measured from voltage traces evoked by injecting a current waveform of the same gain for all recordings (to give a firing rate of ~2–3 Hz). Action potentials were detected by a manually set threshold and the interval between action potentials measured. Dynamic I–V curves were constructed and used to extract a number of parameters including the capacitance, time constant, input resistance, resting membrane potential, spike threshold and spike onset (Fig. 2; [10, 11]). Using these parameters in

a refractory exponential integrate-and-fire (rEIF) model reliably mimics the experimental data, with a spike prediction of ~70–80% as shown previously [10, 11]. All analyses of the dynamic-I–V traces were completed using either MATLAB or Julia software platforms [16].

Recording and analysing miniature excitatory postsynaptic currents (mEPSCs)

AMPA receptor-mediated miniature excitatory postsynaptic currents (mEPSCs) were recorded as previously described [38]. To isolate AMPA-mediated mEPSCs, aCSF contained 1 μM TTX, 50 μM picrotoxin to block GABA_A receptors and 5 μM L689,560 to block NMDA receptors. Recordings of mEPSCs were obtained at a holding potential of -60 mV using an Axon Multiclamp 700B amplifier (Molecular Devices), filtered at 3 kHz and digitised at 20 kHz (Digidata 1440A, Molecular Devices). Data acquisition was performed using pClamp 10 (Molecular Devices). Analysis of mEPSCs was performed using MiniAnalysis software (SynaptoSoft). Events were manually analysed and were accepted if they had amplitude >6 pA (events below this amplitude were difficult to distinguish from baseline noise) and had a faster rise than decay. Statistical significance was measured using a one-way ANOVA.

Extracellular recording of synaptic transmission and plasticity

A 400 μM parasagittal slice was transferred to the submerged recording chamber and perfused with aCSF at 4–6 ml/min (32 °C). The slice was placed on a grid allowing perfusion above and below the tissue and all tubing (Tygon) was gas tight (to prevent loss of oxygen). To record field excitatory postsynaptic potentials (fEPSPs), an aCSF-filled microelectrode was placed on the surface of stratum radiatum in CA1. A bipolar concentric stimulating electrode (FHC) controlled by an isolated pulse stimulator model 2100 (AM Systems, WA) was used to evoke fEPSPs at the Schaffer collateral–commissural pathway. Field EPSPs were evoked every 30 s (0.03 Hz). Stimulus input/output curves for fEPSPs were generated using stimulus strength of 1–5 V for all slices (stimulus duration 200 μs). For the synaptic plasticity experiments, the stimulus strength was set to produce a fEPSP slope ~40% of the maximum response and a 20-min baseline was recorded before plasticity induction. Paired-pulse facilitation was measured over an interval range of 20 to 500 ms. Long-term potentiation (LTP) was induced by high frequency stimulation (HFS, 100 stimuli in 1 s, 100 Hz) and then fEPSPs were recorded for 60 min following LTP induction. Signals were filtered at 3 kHz and digitised on-line (10 kHz) with a Micro CED (Mark 2) interface controlled by Spike software (Vs 6.1, Cambridge

Electronic Design, Cambridge UK). The fEPSP slope was measured from a 1 ms linear region following the fibre volley.

Theta Oscillations

Induction of theta oscillations in CA3

A 400 μM horizontal slice was transferred to an interface recording chamber (Digitimer BSC3) and placed on a mesh support at the interface of an oxygen-rich atmosphere and underlying aCSF. The temperature of the aCSF was set at 31 °C and the flow rate was 1.5 ml/min. An aCSF-filled glass microelectrode was placed in CA3 to record activity. Baseline activity was recorded for 20 min before the bath application of the acetylcholine receptor agonist carbachol, selected to induce oscillations given the evidenced role of acetylcholine receptors in regulating hippocampal-dependent oscillations [7, 123]. Carbachol was applied at 50 μM , a concentration previously demonstrated to induce CA3 theta activity in rodent slices [3, 46, 72, 130]. Theta oscillations were recorded for 30 min with a differential amplifier (Warner instrument DP-301) with filter settings: low pass 3 kHz, high pass 1 Hz, amplification $\times 1000$. Data was acquired at a sampling rate of 10 kHz with a Micro1401 (Cambridge Electronic Design) using Spike 2 software.

Analysis of theta oscillations

Carbachol-elicited oscillations were characterised using power spectral density (PSD) analysis in Spike 2. PSD profiles of the field potential recordings filtered for the theta band (4–7 Hz) were generated by Fourier transform analysis (Hanning window, FFT size 2048, resolution 4.883 Hz). The profiles were calculated from a 100–300 s section of the field potential trace displaying peak oscillatory activity, with the baseline power subtracted offline (Additional file 1: Fig. S2). Recordings from slices from each treatment condition (control, CSF-tau and CSF-tau-depleted) were conducted in a random order each day to prevent any time effects, and a slice was only included in the analysis if robust oscillations were evoked. Differences between the three treatment groups (control, $n=8$; CSF-tau, $n=8$; CSF-tau-depleted, $n=8$) in mean oscillatory power (mV^2) were compared using a Kruskal–Wallis test followed by a Dunn's multiple comparisons test. The peak oscillatory power of each trace ($n=8$ per group) was also compared with the corresponding baseline ($n=8$ per group) within each treatment group and mean differences assessed using Wilcoxon tests. Finally, the mean time period (latency, seconds) from application of carbachol to the onset of oscillatory activity was compared between treatment groups using a Kruskal–Wallis test followed by a Dunn's multiple comparisons test.

Drugs

Picrotoxin (PTX; Sigma), carbachol (carbamoylcholine chloride; Sigma), Tetrodotoxin (TTX; Sigma) and trans-2-carboxy-5,7-dichloro-4-phenylaminocarbonylamino-1,2,3,4-tetrahydroquinoline (L689,560; Hello-Bio) were made up as stock solutions (1–50 mM) in distilled water or dimethyl sulfoxide (DMSO) and then diluted in aCSF on the day of use. The concentration of DMSO did not exceed 0.1% in the final solutions.

Statistical analysis

Statistical analysis was performed using GraphPad Prism. Due to small sample sizes ($n < 15$), statistical analysis was performed using non-parametric methods; Kruskal–Wallis analysis of variance (ANOVA), Mann–Whitney and Wilcoxon signed-rank tests as required. All data are represented as mean and standard error of the mean with individual experiments represented by single data points. For all experiments, significance was set at $p \leq 0.05$. Data points for each experimental condition were derived from a minimum of four individual animals.

Results

Characterisation of CSF-tau before and after the immuno-depletion for tau

To investigate the effects of CSF-tau on neuronal properties, in this proof-of-principle study, we used pooled CSF from multiple de-identified patients. The biomarker profile for the pool was measured with the Lumipulse platform. For the pooled samples used in this study, CSF A β 1-42 level (469 pg/ml) was abnormal as it was below the clinically validated abnormality threshold of 526 pg/ml [50]. A β 1-42/A β 1-40 ratio was also in the positivity range (< 0.072 pg/ml). T-tau (measured = 542 pg/ml) was above the abnormality threshold of 409 pg/ml [82] but p-tau181 remained negative [50]. These profiles suggest that pooled CSF sample was amyloid-positive, phosphorylated-tau-negative but neurodegeneration-positive (A + T-N+) [69].

To allow determination of the specific effects of tau on electrophysiological properties, an aliquot of the pooled CSF-tau sample was immuno-depleted for tau by the simultaneous application of the monoclonal antibodies Tau12, HT7 and TauAB (epitopes: amino acids 6–18, 159–163 and 425–441 respectively) that together cover a wide span of the tau-441 protein sequence. To confirm that tau removal protocols were effective, the immuno-depleted samples were reanalysed for t-tau, p-tau181 and ptau-231 using Simoa assays. P-tau181, p-tau231 and total-tau signals decreased by 86.9% and 92.4% and 83.8%, respectively. To further validate the depletion, p-tau181 was measured using a fully automated Lumipulse platform and the signal decreased by 80.5% (Fig. 1).

CSF-tau enhances hippocampal pyramidal neuronal excitability

Tau aggregates have previously been reported both in vitro and in vivo to affect neuronal function, excitability, and synaptic plasticity [20, 45, 61, 81, 105, 108]. These tau-mediated deficits are largely mediated by soluble forms of the protein [61, 96, 115, 129], including those isolated from AD brains [80, 81]. However, studies using patient-derived CSF samples, which are estimated to contain a fraction of the soluble tau aggregates from AD brains [73, 90, 110], are lacking. Here, we investigated if the reported pathological effects of soluble tau aggregates can be reproduced with CSF-tau.

In this study, we used pooled CSF samples from multiple patients. The relatively large volume of pooled sample (5 ml) allowed us to perform a wide range of experiments using the same sample to fully characterise its neurotoxic effects. We diluted the CSF-tau sample with aCSF to reduce the volume of sample that was required for each experiment. As our eventual end goal will be to use individual patient samples (much smaller volumes ~ 300 μ l) to enable correlation with clinical data, we first sought to find the minimum volume (maximum dilution in aCSF) of CSF-tau, for which we could detect a change in neuronal function. We tested 1:100, 1:30 and 1:15 dilutions of the CSF-tau in aCSF ($n = 8$ per group). We used neuronal excitability, measured using whole-cell patch clamp recording from single CA1 pyramidal cells in the hippocampus, as the functional readout. We have previously found this to be a reliable and robust change induced by recombinant tau [60, 61]. We found no significant changes to neuronal excitability with either the 1:100 dilution or 1:30 dilution of CSF-tau, but a significant depolarisation and increase in firing rate was observed with a 1:15 dilution (100 μ l CSF in 1.5 ml aCSF; Additional file 1: Fig. S1). We therefore used a 1:15 dilution of CSF-tau and CSF-tau-depleted for all subsequent experiments. It has previously been demonstrated that undiluted human CSF can alter neuronal properties [17]. Therefore, in this set of pilot experiments, we also validated that, at the 1:15 dilution that we are using, there was no effect on neuronal properties (measured as resting membrane potential and firing rate as a correlate of neuronal excitability) when slices were incubated with CSF from a control 62-year-old female patient with no detectable amyloid and tau pathology (Additional file 1: Fig. S1).

To fully evaluate the effects of CSF-tau at a single neuron level, slices were either incubated with CSF-tau ($n = 11$), CSF-tau-depleted ($n = 10$) or control aCSF ($n = 10$; no human sample) for 1 h before recordings were made. Initially, standard current step protocols were used to measure passive neuronal parameters (see

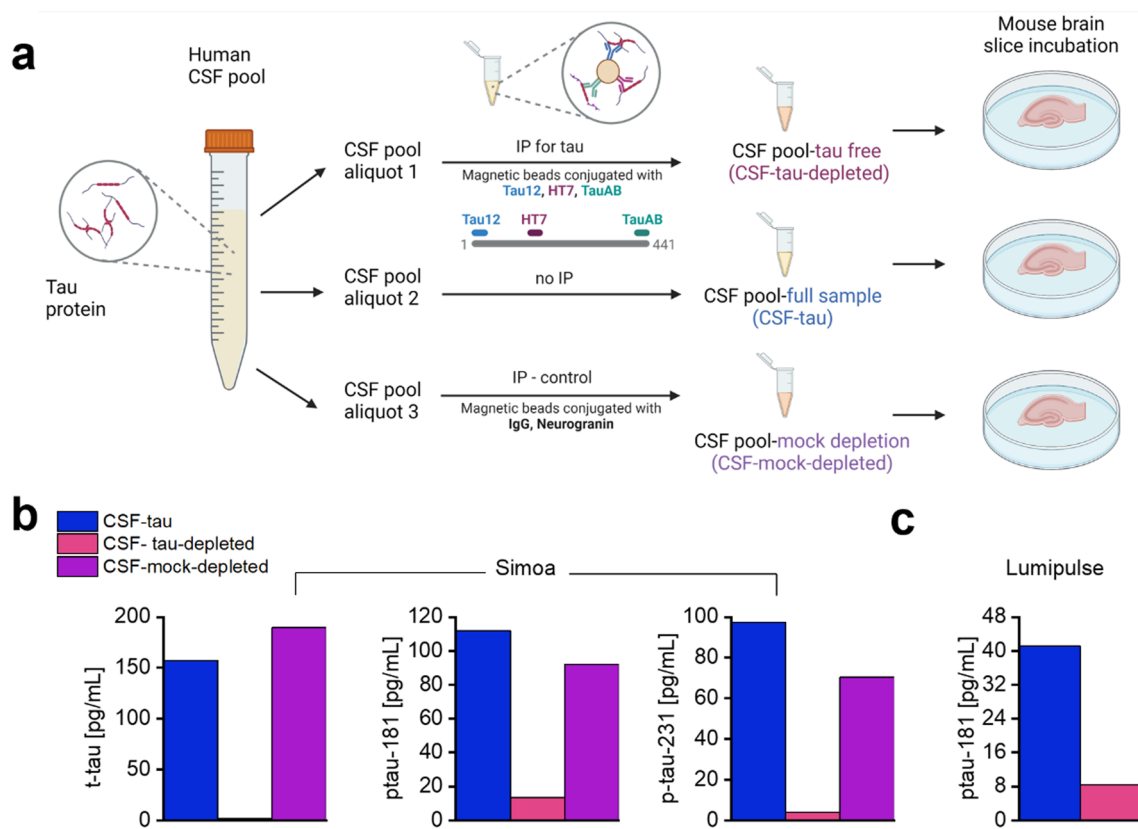


Fig. 1 Immunodepletion of pooled CSF to remove tau using a combination of antibodies targeting the N terminus, mid region, and C terminus of tau. **a**, Pooled human CSF from multiple de-identified patients (CSF-tau) was divided into 3 aliquots. An aliquot of the pooled CSF-tau sample was immuno-depleted for tau by the simultaneous application of the monoclonal antibodies Tau12, HT7 and TauAB (epitopes: amino acids 6–18, 159–163 and 425–441, respectively) that together cover nearly the entire tau-441 protein sequence using published protocols [79], this is referred to herein as CSF-tau-depleted. The second aliquot remained the full sample, referred to as CSF-tau. The final aliquot underwent the same immunodepletion protocol with different antibodies (anti-mouse IgG and neurogranin (H-6) antibody) to provide a control for the tau immunodepletion, referred to as CSF-mock-depletion. **b**, To verify the removal of tau after the immuno-depletion in aliquot 1, t-tau assay from Quanterix, p-tau181 [75] and p-tau231 [8] in house assays were used for tau measurements in the CSF-depleted and non-depleted aliquots and compared in parallel against the CSF-mock-depleted sample on a Simoa HD-X instrument (Quanterix, Billerica, MA, USA) following methods originally described in the cited publications. **c**, The immunodepletion of tau was further validated by comparison to the full CSF sample using fully automated Lumipulse (Fujirebio) platform following published protocols [49]

materials and methods for details). Incubation with CSF-tau led to significant depolarisation of the resting membrane potential (RMP; mean RMP in control slices of -68 ± 0.92 mV compared to the mean RMP in CSF-tau of -63 ± 0.79 mV; Fig. 2a, b, c), an effect that was not observed in slices incubated in CSF-tau-depleted (mean RMP of -69 ± 1.09 mV; Fig. 2a, b, c). A Kruskal–Wallis test showed that the difference in RMP between the three treatment groups was significant (Fig. 2c; $H(2) = 14.98$, $p < 0.0006$), with Dunn’s tests revealing a significant depolarisation of the RMP following CSF-tau treatment relative to aCSF control slices ($p < 0.0121$) and treatment with CSF-tau-depleted ($p < 0.0008$), whilst there was no significant difference between control and CSF-tau-depleted groups ($p > 0.9999$).

Incubation with CSF-tau also significantly increased the input resistance (IR, reflecting a decrease in whole cell conductance). The mean IR in control slices was 143.6 ± 5.2 M Ω , compared to the mean IR in slices incubated in CSF-tau of 167 ± 7.2 M Ω ; Fig. 2a, b, d), an effect which again was not observed in slices incubated in CSF-tau-depleted (mean IR of 126 ± 9.9 mV; Fig. 2a, b, d). The difference in IR between the three treatment groups was also significant (Kruskal Wallis test; Fig. 2d; $H(2) = 12.39$, $p < 0.0020$), with Dunn’s tests revealing a significant increase in IR following CSF-tau treatment relative treatment with CSF-tau-depleted ($p < 0.0013$), whilst there was no significant difference between either control (aCSF) and CSF-tau-depleted groups ($p < 0.2831$).

Given that CSF-tau depolarises the resting membrane potential and increases the IR, we predicted that it should also increase the action potential firing rate. To test this, we used a 40 s fluctuating naturalistic current injection (to mimic synaptic activation) and measured the firing rate. Incubation with CSF-tau significantly increased firing rate (FR). The mean FR in control was 2.3 ± 0.5 Hz compared to the mean FR in neurons exposed to CSF-tau of 4.2 ± 0.6 Hz; Fig. 2e, f). This increase in FR was not observed in slices incubated in CSF-tau-depleted (mean FR of 2.1 ± 0.3 Hz; Fig. 2e, f). A Kruskal–Wallis test showed that the difference in FR between the three treatment groups was also significant (Fig. 2f; $H(2) = 10.4$, $p < 0.0055$), with Dunn's tests revealing a significant increase in FR following CSF-tau treatment relative to aCSF control slices ($p < 0.0129$) and treatment with CSF-tau-depleted ($p < 0.0222$), whilst there was no significant difference between control and CSF-tau-depleted groups ($p > 0.9999$).

We have previously shown that tau aggregates decrease the rheobase (minimum current needed to fire an action potential; [60]), therefore we next checked whether the increase in excitability was accompanied by a change in rheobase (Fig. 2g, h). The mean rheobase in neurons exposed to CSF-tau was significantly decreased (52 ± 6.6 pA) compared to aCSF control slices (87 ± 6.8 pA) or slices incubated in CSF-tau-depleted (74 ± 6.9 pA). A Kruskal–Wallis test showed that the difference in rheobase between the three treatment groups was also significant (Fig. 2h; $H(2) = 9.3$, $p < 0.0093$), with Dunn's tests revealing a significant decrease in rheobase following CSF-tau treatment relative to aCSF control slices ($p = 0.0080$), whilst there was no significant difference between aCSF control and CSF-tau-depleted groups ($p = 0.8856$).

To determine if other neuronal parameters were significantly altered by CSF-tau, we used the dynamic IV method [10, 11] to measure capacitance, the time constant, the spike threshold and spike onset. Unlike our previous studies, using recombinant tau oligomers and associated truncations [60, 61], there were no significant

differences in any of these parameters. We also evaluated whether there were changes to action potential amplitude or half-width, which we have previously observed with recombinant soluble tau aggregates [60, 61]. Again, we observed no significant changes to either of these parameters between the three conditions.

Thus, CSF-tau replicates a number of the pathological effects which have been reported previously in models of tauopathy. These effects were absent when tau was removed by immunodepletion, indicating that tau is critical to these disease-associated changes.

CSF-tau enhanced basal fEPSP amplitude and paired pulse facilitation and long-term potentiation

Next, we investigated whether the changes to neuronal excitability in single pyramidal cells were accompanied by changes in synaptic transmission and plasticity in the CA1 region of the hippocampus.

Incubation in CSF-tau led to increased basal synaptic transmission, as measured by stimulus input/output curves (Fig. 3a, b). For example, the mean fEPSP slope at 3 V in CSF-tau treated slices was 0.46 ± 0.06 mV/ms ($n = 8$) compared to control slices which was 0.25 ± 0.04 mV/ms ($n = 10$) and 0.22 ± 0.03 mV/ms in CSF-tau-depleted ($n = 12$). A two-way ANOVA evaluating the fEPSP response to increasing stimulus across the three conditions showed a significant difference between the groups ($F(25, 225) = 15.05$, $p < 0.0001$) with significantly greater fEPSP slope for CSF-tau compared to CSF-tau-depleted at 2.5 mV ($p = 0.0486$), 3 mV ($p = 0.0241$) and 3.5 mV ($p = 0.0494$) stimulus strengths. We also measured the fibre volley for a given stimulus (4 mV) it found that it was significantly larger in CSF-tau (0.29 ± 0.03 mV) compared to control (0.15 ± 0.02 mV, $p = 0.0278$).

We then examined whether there were changes to paired pulse facilitation (PPF). If the increase in fEPSP amplitude is a consequence of an increase in release probability, then it would be predicted that the degree of PPF would be reduced. However, the opposite was observed, and the degree of facilitation was

(See figure on next page.)

Fig. 2 CSF-tau enhances hippocampal pyramidal neuronal excitability. **a.** Representative examples of standard current–voltage responses for slices that have been incubated in control aCSF (light blue; $n = 10$), CSF-tau (CSF; dark blue; $n = 11$) or CSF-tau immunodepleted for tau (CSF-depleted; Pink; $n = 10$). See Materials and Methods for incubation protocols. CSF-tau depolarised the resting membrane potential of the recorded neurons. **b.** The most negative step from traces in (a), clearly highlighting that CSF-tau also mediates an increase in input resistance. **c.** CSF-tau incubation resulted in a significant depolarisation of the resting membrane potential ($p < 0.0006$), which was not observed in the CSF sample immuno-depleted for tau. **d.** CSF-tau incubation also significantly increased input resistance ($p < 0.0020$), an effect which was also not observed in the CSF sample that was immunodepleted for tau. **e.** Representative example of membrane-potential responses to naturalistic current injection for each of the three conditions. **f.** CSF-tau significantly increased the firing rate (a correlate of neuronal excitability; $p < 0.0055$). No change was observed with the CSF-tau sample immunodepleted for tau compared to control. **g.** The rheobase current (minimal current to evoke an AP) was determined by injecting a current ramp (–50 to 200 pA) and measuring the minimum current required to fire an action potential. **h.** CSF-tau incubation significantly decreased the rheobase ($p = 0.0093$). Panels a, b, e and g show representative example traces and c, d, f and h show the mean data and SEM, with individual datapoints overlaid

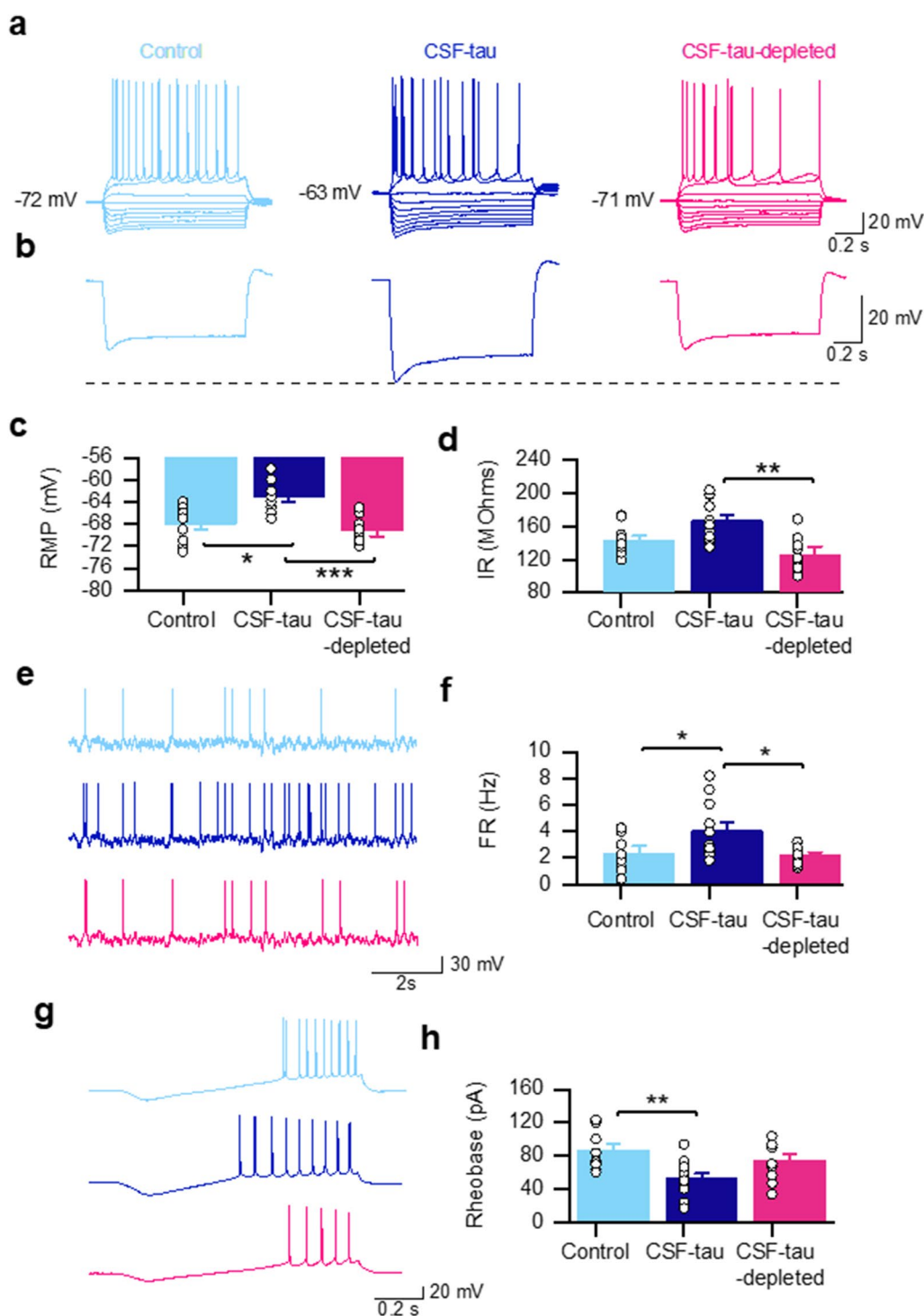


Fig. 2 (See legend on previous page.)

significantly increased at 100 ms and 200 ms intervals (Fig. 3c, d). For example, the mean paired-pulse ratio at a 100 ms interval in CSF-tau was 2.23 ± 0.1 compared to control aCSF which was 1.94 ± 0.07 and 1.87 ± 0.04 in CSF-tau-depleted. A two-way ANOVA evaluating the

paired-pulse ratio at different intervals across the three conditions showed a significant difference between the groups ($F(2, 135) = 10.62, p < 0.0001$) with significantly greater facilitation for CSF-tau compared to

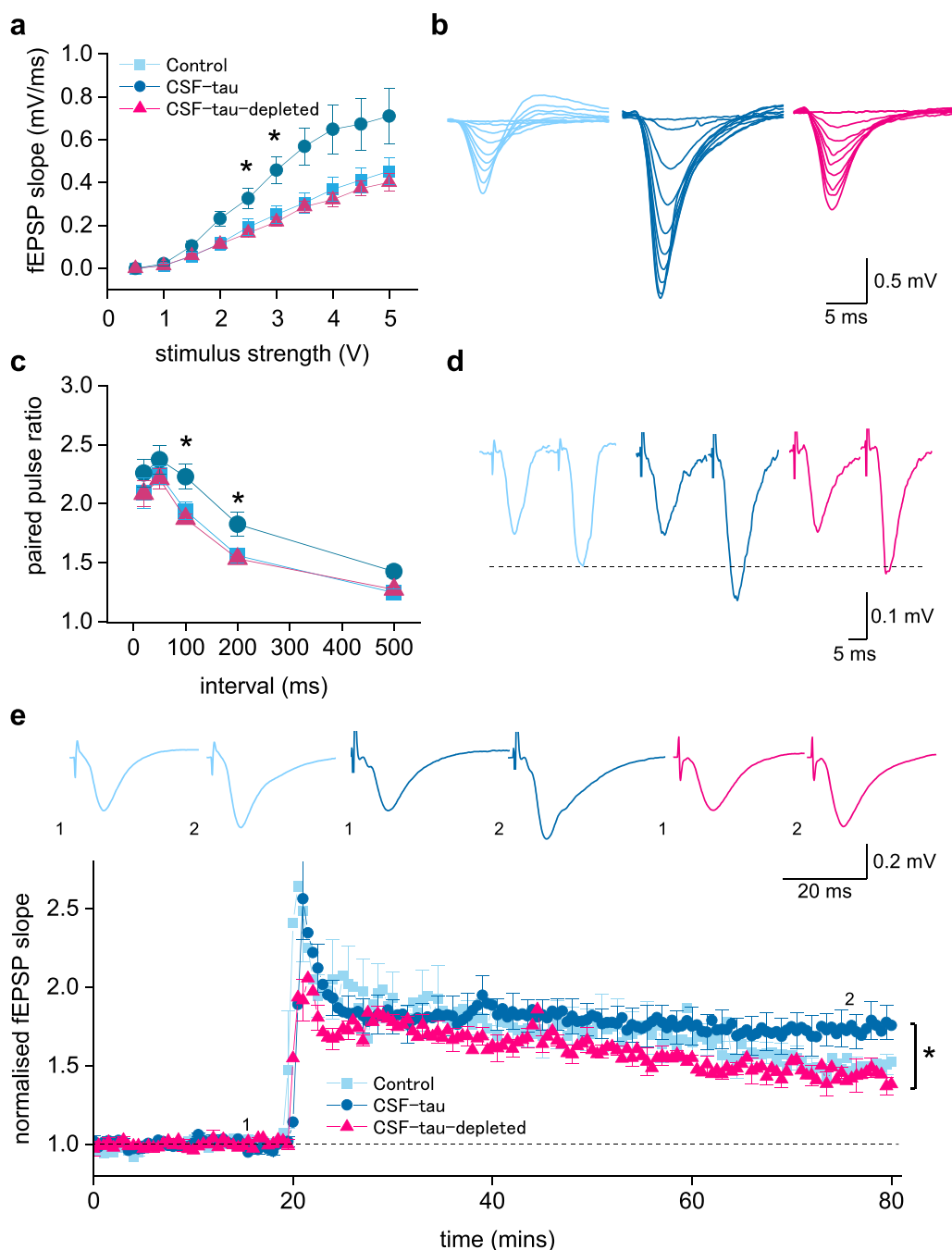


Fig. 3 CSF-tau enhances basal synaptic transmission and synaptic plasticity. **a.** Graph plotting mean fEPSP slope against stimulus strength for control (n = 10 slices), CSF-tau (n = 11 slices) and CSF-tau-depleted (n = 10 slices). **b.** Superimposed fEPSP waveforms at increasing stimulus strengths (0.5 to 5 V) for each of the three conditions. CSF-tau significantly enhanced fEPSP slope. **c.** Graph plotting mean paired pulse ratio against interval for all three conditions. CSF-tau significantly enhanced paired pulse facilitation. **d.** Representative example traces of fEPSP waveforms for the 200 ms interval for all three conditions. The first fEPSPs have been normalised in this figure so that facilitation can be compared across conditions. **e.** Graph plotting mean normalised (to the baseline) fEPSP slope against time for all three conditions. After a 20-min baseline, LTP was induced by HFS. Inset, example fEPSP waveforms before and after LTP induction (average of waveforms at 75–80 min). The mean potentiation was enhanced in CSF-tau. All Data is represented as Mean ± SEM

CSF-tau-depleted at 100 ($p=0.0081$) and 200 ms time intervals ($p=0.0368$).

In the same recordings, we then examined whether CSF-tau altered long-term synaptic plasticity by recording long term potentiation (LTP) at the CA1 Schaffer collateral synapses. We measured the potentiation 60 min after HFS [63, 137] and found LTP to be significantly enhanced by CSF-tau. The mean potentiation (displayed as normalised fEPSP slope, Fig. 3e) at 55–60 min after induction was 1.76 ± 0.09 in CSF-tau, in control aCSF it was 1.51 ± 0.06 and in CSF-tau-depleted it was 1.46 ± 0.07 . A Kruskal–Wallis test showed that the difference in potentiation between the three treatment groups was significant ($H(2)=6.683$, $p=0.0354$) with Dunn's tests revealing a significant increase in potentiation following CSF-tau treatment relative to treatment with CSF-tau-depleted ($p=0.0415$), whilst there was no significant difference between control and CSF-tau-depleted groups ($p>0.9999$).

Incubation with CSF-tau leads to an increase in the amplitude and frequency of mEPSCs

Since the increase in fEPSP amplitude did not appear to result from an increase in release probability, we hypothesised that it could result from an increase in synaptic AMPA receptor density. To evaluate whether there are changes in postsynaptic AMPA receptor currents, we used whole-cell voltage clamp recordings from CA1 pyramidal neurons to record AMPA receptor-mediated miniature EPSCs (mEPSCs) in the presence of PTX (to block GABA_A receptors), L689,560 (to block NMDA receptors) and TTX (to block voltage-gated Na channels).

We observed a significant increase in the frequency of mEPSCs (shorter interval between events) in the slices incubated with CSF-tau compared to control slices (Fig. 4a). The distribution of intervals between events in CSF-tau was significantly different to that of control slices (Kolmogorov–Smirnov test; $D=0.5494$, $p<0.0001$, Fig. 4b) with mEPSCs occurring at a much higher frequency in CSF-tau treated slices ($n=800$ pooled mEPSCs from 8 slices). On average the frequency was increased 7.5-fold compared to control recordings ($n=600$ mEPSCs from 6 slices). This effect was partially reversed with CSF-tau-depleted ($n=800$ pooled mEPSCs from

8 slices; Kolmogorov–Smirnov test CSF-tau-depleted vs CSF-tau; $D=0.1441$, $p<0.0001$, Fig. 4b), but not fully prevented, suggesting either that very low levels of tau can produce this effect, or some other component in the CSF is responsible. Then, by comparing the mean mEPSC intervals between events for each slice across the three conditions, we further validated that slices incubated in CSF-tau showed significantly decreased intervals between events (increased frequency) compared to control slices (mean interval in CSF-tau was 1.9 ± 0.09 s vs mean interval in control was 17.6 ± 1.04 s; Fig. 4c). A Kruskal–Wallis test showed that the difference in intervals between the three treatment groups was significant (Fig. 4c; $H(2)=12.62$, $p=0.0003$), with Dunn's tests revealing a significant decrease in interval following CSF-tau treatment relative to aCSF control slices ($p=0.0015$) and CSF-tau-depleted vs control aCSF ($p=0.0293$).

We also found that the amplitude of mEPSCs was significantly enhanced in CSF-tau incubated slices (Fig. 4d). Using a Kolmogorov–Smirnov test to compare the cumulative frequency of the pooled mEPSCs for each of the conditions, we found that distribution of mEPSC amplitudes in slices exposed to CSF-tau was significantly higher than those in control slices ($D=0.1533$, $p<0.0001$) and to slices incubated with CSF-tau-depleted ($D=0.1441$, $p<0.0001$), indicating that depletion for tau prevents the effects. Then, by comparing the mean mEPSC amplitudes for each slice across the three conditions, we further validated that slices incubated in CSF-tau showed increased amplitudes compared to control slices (mean amplitude in CSF was 22.5 ± 0.39 pA vs mean amplitude in control was 18.9 ± 0.33 pA; Fig. 4e). A Kruskal–Wallis test showed that the difference in amplitudes between the three treatment groups was significant (Fig. 4e; $H(2)=12.85$, $p=0.0002$), with Dunn's tests revealing a significant increase in amplitude following CSF-tau treatment relative to aCSF control slices ($p=0.0015$) and CSF-tau compared to CSF-tau-depleted slices ($p=0.0026$).

Finally, to establish whether there were any changes to the kinetics of the mEPSCs, we then measured the rise and decay time for the average waveform from each recording. The rise time was measured (10–90%) and the decay time was obtained by fitting with a single

(See figure on next page.)

Fig. 4 CSF-tau increases the frequency and amplitude of AMPA receptor-mediated mEPSCs. **a**, Representative traces (10 s duration) from control, CSF-tau and CSF-tau depleted incubated slices, demonstrating the significant difference in mEPSC frequency and amplitude. **b**, Cumulative frequency plot of mEPSC interval (between events). **c**, Mean mEPSC interval for each slice is plotted. CSF-tau decreases the interval between mEPSCs, representing an increase in frequency, compared to control ($p=0.0004$). **d**, Cumulative frequency plot of mEPSC amplitude. **e**, Mean mEPSC amplitude for each slice is plotted. CSF-tau significantly enhances the amplitude of mEPSCs compared to control ($p=0.0225$) and CSF-tau-depleted ($p=0.0026$). **f, g**, The average mEPSC waveforms for each recording were analysed for kinetics (10–90% for the rise time and exponential fit for the decay time). An example is shown for control (f) and CSF-tau (g), and the exponential fit is overlaid in black. Inset, higher magnification to show the decay fit. Data is represented as Mean \pm SEM

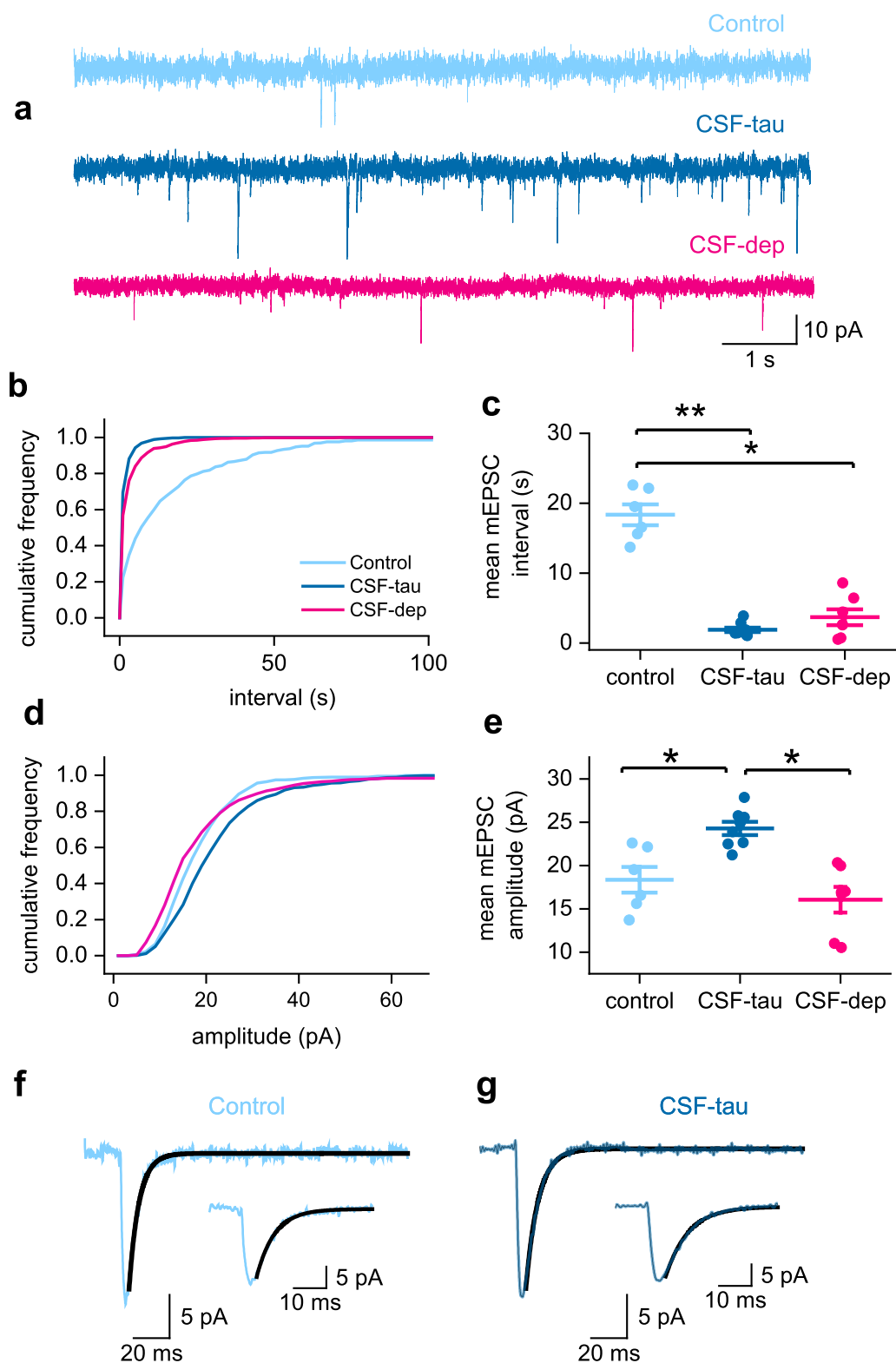


Fig. 4 (See legend on previous page.)

exponential. There was no change to rise or decay kinetics between the three conditions.

CSF-tau alters the generation and maintenance of theta oscillations

We have found that CSF-tau markedly changes neuronal properties, synaptic transmission, and synaptic plasticity. We have next investigated how these changes can lead to alterations in emergent network activity. Hippocampal hyperexcitability has been identified in AD patients prior to the onset of cognitive symptoms and is associated with increased oscillatory power in theta bands relative to control or MCI groups [47, 66, 92, 93, 101, 112, 114]. Thus, changes in theta power are of interest as a potential predictor for the development of AD [70].

Bath application of the acetylcholine receptor agonist carbachol (50 μ M) induced robust, reliable theta oscillations, as demonstrated by Wilcoxon tests comparing peak oscillatory amplitude and baseline activity for all three treatment groups (Fig. 5a–c). In control slices pre-incubated with aCSF (Fig. 5a), there was a significant difference between baseline power and oscillatory power ($W = -32$, $p = 0.0234$). In slices pre-incubated with CSF-tau (Fig. 5b), the difference between baseline power and oscillatory power was also significant ($W = -36$, $p = 0.0078$). Finally, in slices preincubated with CSF-tau-depleted (Fig. 5c), there was a significant difference between baseline power and oscillatory power ($W = -36$, $p = 0.0078$). A Kruskal–Wallis test showed that the difference in peak oscillatory power between the three treatment groups was also significant (Fig. 5d; $H(2) = 11.02$, $p = 0.0041$), with Dunn's tests revealing a significant increase in theta power following CSF-tau treatment relative to aCSF control slices ($p = 0.0194$) and treatment with CSF-tau-depleted ($p = 0.008$), whilst there was no significant difference between control and CSF-tau-depleted groups. The significant enhancement in the amplitude of hippocampal theta oscillations following incubation with CSF-tau aligns with previous published studies demonstrating that increased theta power is one of the first pathological changes observed in AD patients [14, 33, 37, 71, 92, 94]. Finally, the time to onset of oscillatory activity was also significantly different between groups (Fig. 5e; $H(2) = 10.09$, $p = 0.0065$), with CSF-tau slices showing a significantly quicker onset of oscillations relative to control ($p = 0.005$) following carbachol application.

Validation of tau effects using CSF-mock-depleted.

To further demonstrate that the observed effects were a result of tau and not an artefact of the immunodepletion protocol, we used an aliquot of the CSF pool, immunodepleted using the same protocol but with

antibodies against IgG and neurogranin (CSF-mock-depleted). We compared this against control aCSF, and the data collected with the CSF-tau (full sample) and CSF-tau-depleted (depleted for tau), see Additional file 1: Fig. S3. We found that slices incubated with CSF-mock-depleted resulted in a significant depolarisation of the resting membrane potential compared to control (aCSF) ($p = 0.0018$) and compared to CSF-tau-depleted ($p = 0.0001$) and was not significantly different from incubation with the full CSF-tau sample. It also resulted in a significant increase in firing rate compared to control (aCSF) ($p = 0.0109$) and compared to CSF-tau-depleted ($p = 0.0481$) and was not significantly different from incubation with the full CSF-tau sample. We also evaluated the effect of slice incubation with the CSF-mock-depleted sample on carbachol-induced theta oscillations in the CA3 region of the hippocampus. A Kruskal–Wallis test showed a significant difference in peak oscillatory power between control, CSF-tau, CSF-tau-depleted and CSF-mock-depleted groups ($H = 18.34$, $p = 0.0004$). Dunn's multiple comparison tests demonstrated that CSF-mock-depleted slices had significantly stronger oscillatory power compared to control (aCSF; $p = 0.0183$) and CSF-tau-depleted slices ($p = 0.0012$) and were not significantly different from the CSF-tau (full) group, see Additional file 1: Fig. S3.

Discussion

CSF biomarkers for tau and phosphorylated-tau have proved to be reliable predictors/indicators of AD [19, 74]. Tau-based biomarkers can differentiate AD from unaffected individuals and other tauopathies with strong predictive values [74]. Moreover, tau-based biomarker levels change in a stepwise manner across the AD spectrum, allowing for more accurate disease staging, clinical diagnosis, as well as clinical trial recruitment and monitoring [74]. Pathological tau species in AD brains are post-translationally modified, including being phosphorylated and aggregated both in soluble (e.g., oligomers, protomers) and insoluble (neurofibrillary tangles) forms. We currently have high-performing biomarkers that reflect both phosphorylation (e.g., p-tau181) [76] and aggregation [64, 116] of tau in CSF. However, little is known about the toxic effects on brain function of these soluble tau forms in CSF, and this could shed new light on the novel biomarkers developed and applied clinically.

The pathological effects of soluble tau aggregates have been studied extensively in animal models [20, 45, 81, 105, 108]. These changes are normally induced by full-length soluble aggregated forms of tau, mostly produced recombinantly [6, 34, 61, 88]. However, recent work has suggested that tau aggregates produced *in vitro* do not recapitulate the structural features of authentic AD brain

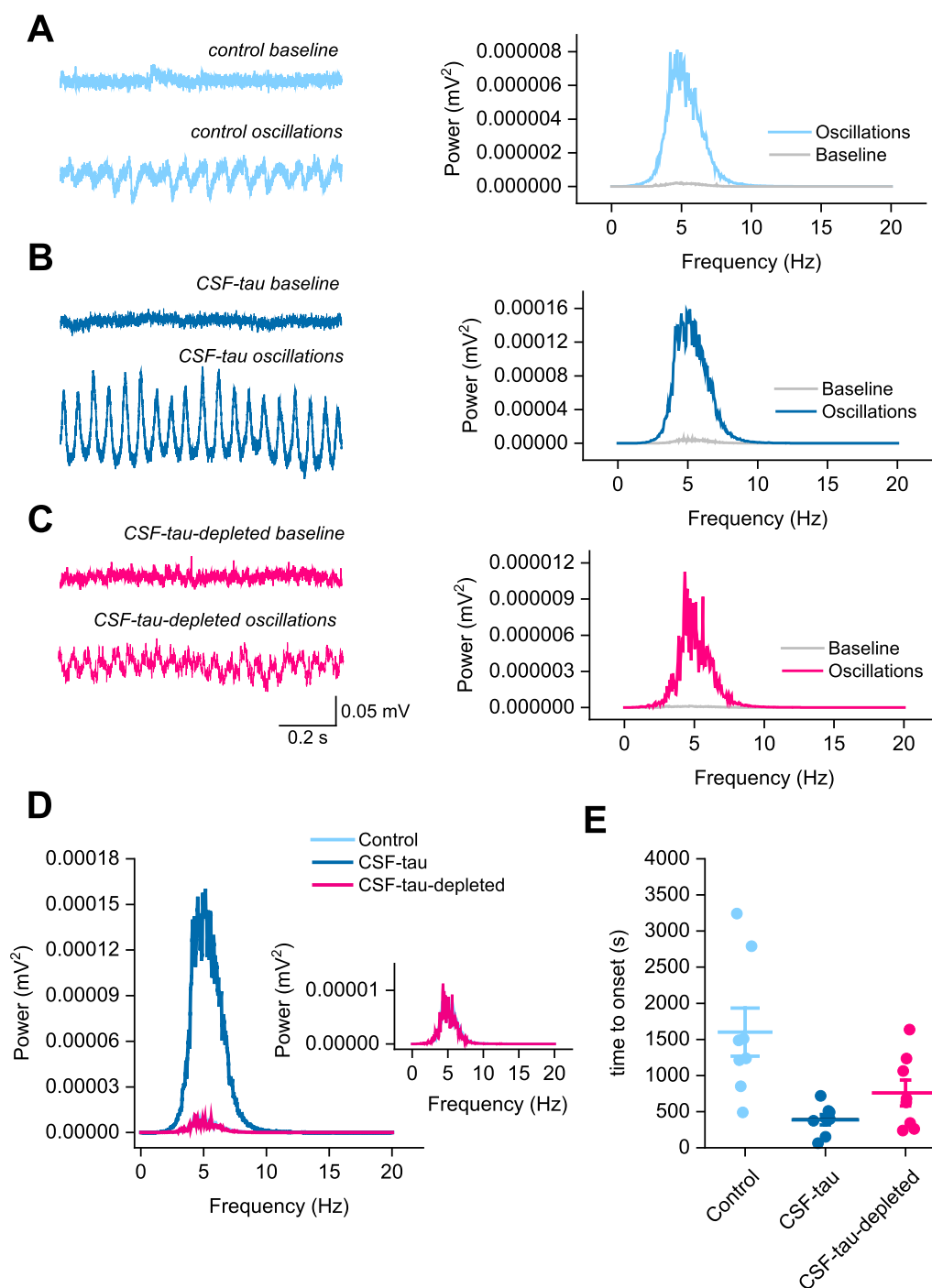


Fig. 5 CSF-tau alters the generation and amplitude of theta oscillations. Theta oscillations in the CA3 region of the hippocampus were recorded in an interface chamber (see methods for details). Bath application of carbachol (50 μ M) in this study induced robust, reliable theta oscillations across all three experimental conditions (**a, b, c**). **Left**, Representative examples of baseline and theta oscillations for each of the three conditions. **Right**, Power spectrum from the representative example confirming the oscillations to be in the theta range (4–7 Hz). **d**, mean power spectrums for each of the conditions. CSF-tau incubated slices had significantly stronger oscillatory power compared to control or CSF-tau-depleted incubated slices ($P < 0.0001$). Inset, higher magnification of control and CSF-tau-depleted traces. **e**, CSF-tau incubated slices also showed a significantly quicker onset of oscillatory activity relative to control ($p = 0.005$). Data is presented as Mean \pm SEM

tau [136]. We therefore sought to investigate if tau in CSF, which is often found in truncated forms [32], modulates neuronal function.

To do this, we incubated acute brain slices from male and female wildtype C57/BL6 3–4-week-old mice with biomarker-quantified tau-positive CSF pooled from multiple patients. We decided to use this age of mouse to ensure that there would be no deficits in the hippocampal neural circuitry (as opposed to using aged mice) where variability between recordings is much higher and thus our baseline parameters would be consistent. Therefore, any changes induced by the CSF-tau would be easy to detect. As the goal for future studies is to scale down the volume of sample from pooled samples (5 ml in this study) to individual patient samples (~300 μ l), to enable correlation with clinical data, we first determined the minimum volume of CSF-tau (diluted in aCSF) for which we could detect a change to neuronal function. We then performed a suite of electrophysiological tests to evaluate the effect on neuronal and network function. We demonstrate that CSF-tau markedly increases neuronal excitability, alters synaptic transmission and plasticity, and modifies the generation and maintenance of hippocampal theta oscillations.

In our experiments, the human CSF was diluted 1:15 in aCSF for slice incubation, which is equivalent to 66 μ l of CSF and 934 μ l of aCSF (for a total volume of 1 ml), with no human CSF present during recording. Thus, it is extremely unlikely any small changes in the ionic composition of the aCSF plus human aCSF or the presence of neurotransmitters (see [17]) would have any effect on the measured electrophysiological parameters. This was confirmed by the results of two experiments: (1) by the lack of effect of CSF-tau-depleted on neuronal and network function and (2) by no effect of control CSF taken from an individual with no detectable amyloid and tau pathology.

Immunodepletion of CSF pool to remove tau species

A wide range of tau fragments can be found in CSF. These are mostly N-terminal to mid-domain tau fragments and provide good biomarkers for disease prognosis, diagnosis, and staging [19, 111]. For this reason, in this study we have used a combination of three antibodies to provide a robust removal of N-term and Mid-terminal tau species: Tau12 N-terminal [epitope=amino acids 6–18], HT7 mid-region [epitope=amino acids 159–163], and TauAB C-terminal antibody [epitope=amino acids 425–441]. To verify the removal of tau after the immunodepletion, we used different assays that cover various longer (Simoa t-tau assay from Quanterix and p-tau181 [75] and p-tau231 [8] in house assays) and shorter (Lumi-pulse p-tau181 assay [82]) tau fragments, respectively.

Although less abundant, recent studies have shown evidences of other tau fragments in CSF, including microtubule-binding region (MTBR)-containing species [64, 65]. In this initial study, we did not include antibodies specifically targeting the MTBR of tau. Therefore, we cannot guarantee the extent of removal of this region of the protein. However, we demonstrate significant reduction of total and phospho-tau and significant rescue of the functional effects on neuronal function and oscillations when tau is removed. To validate that the immuno-depletion process did not have effects (other than the removal of tau) that could contribute to observed changes, an aliquot of the full CSF pool underwent the same immuno-depletion process with a bead cocktail conjugated with anti-mouse IgG (GE healthcare) and neurogranin (H-6, Santa Cruz Biotechnology) antibodies, providing a 'mock-depletion' control. CSF-mock-depleted displayed comparable changes to neuronal and network function as the full sample and was significantly different to both CSF-tau-depleted and control aCSF for all measured parameters, confirming that the effects are not an artifact of immunodepletion. Thus, the observed changes can be attributed to CSF-tau. Additional studies using different antibody panels are nevertheless planned in order to expand on our findings. While we cannot be certain that all of the observed effects are due solely to tau, as it may exist as a complex with other proteins, we can conclude that, as immuno-depleting for tau abolished the effects, tau must play a central role in mediating the changes.

CSF-tau led to an increase in excitability and decrease in whole-cell conductance

We used both standard IV (with step current injections) and the DIVs (with naturalistic current injection) to extract neuronal parameters. In slices incubated with CSF-tau, both approaches for parameterisation measured a marked decrease in whole-cell conductance (rise in neuronal input resistance) and a depolarisation of the resting membrane potential leading to an increase in firing rate (a correlate of neuronal excitability). Obtaining comparable results using two independent methods for the extraction of neuronal parameters strengthens the robustness of this observation.

Depolarisation of the resting membrane potential and neuronal hyperexcitability are consistent with previously reported data in numerous tauopathy models [61, 108, 122, 132], for example in the rTg4510 mouse model, which expresses human tau variant P301L, where the pyramidal cells were depolarised by ~8 mV compared to WT littermates [108]. The increase in input resistance and firing rate, coupled with the observed depolarisation could result from the block of a standing (or leakage) conductance for example a two-pore-domain potassium

(K2P) channels that contribute to maintaining the resting potential [87]. A comparable increase in neuronal hyperexcitability has also been observed in AD patients in individuals performing memory-encoding tasks [28, 41, 56]. This phenotype is observed in the early stages of disease, before pronounced cell loss and hypoactivity [12, 48]. Thus, our *in vitro* findings compliment the published literature both for animal models and for early AD when measured in patients [12, 48].

CSF-tau enhanced synaptic transmission and plasticity

Soluble tau aggregates have been shown to alter synaptic plasticity both in *in vitro* and *in vivo* models of tauopathy [1, 45, 105, 107]. Therefore, we next investigated if CSF-tau altered synaptic plasticity by measuring paired pulse facilitation (PPF) and long-term potentiation (LTP). In slices incubated with CSF-tau, we observed enhanced basal transmission (as measured from input–output curves). In slices incubated with CSF-tau, we observed enhanced input–output responses. If this was solely due to an increase in release probability, one might expect that there would be less paired pulse facilitation, however, this is not what we observed. Slices incubated with CSF-tau showed significantly enhanced paired pulse facilitation (PPF). The mechanism for the enhancement of PPF is not clear but is unlikely to result from changes in GABAergic transmission, since blocking either GABA_A or GABA_B receptors has no effect on PPF at CA1 synapses [83]. One could speculate that CSF-tau modulates intracellular Ca²⁺ levels and that elevated levels of Ca²⁺ (following the first stimulus) persist for longer durations in neurons exposed to CSF-tau. Thus, facilitation would remain elevated at longer inter-pulse intervals, without effecting the PPF at short intervals. This seems a plausible hypothesis as tau has been linked to changes in intracellular Ca²⁺ [39, 120].

As well as observing enhanced PPF, we also observed an increase in LTP magnitude in slices that had been incubated in CSF-tau. Since the baseline fEPSP slope was set to 40–50% maximum, to ensure an equal range for potentiation across the experimental groups, the slope of baseline fEPSPs will have been larger in the CSF-tau group. This could potentially lead to enhanced LTP, since there will be greater synaptic activation, we will look to test this in future studies.

We then recorded AMPA receptor-mediated mEPSCs. In slices incubated with CSF-tau, we observed significant increases in both the amplitude and frequency of mEPSCs. Depletion of tau markedly reduced, but did not abolish, the effects of CSF on mEPSC frequency. Thus, either very low levels of tau can produce this effect, or some other component in the CSF is responsible. This will be explored further in future studies. An increase in

mEPSC frequency would suggest an increase in release probability, consistent with the increased input–output responses, which could result from an increase in the number of active zones or the number of docked vesicles [9, 100, 135]. The increase in mEPSC amplitude could reflect an increase in the number of postsynaptic receptors, altered vesicle size or an increase in the number of synapses if the mEPSCs are multiquantal [68, 86, 135]. It is also possible that synapses that were previously silent (exhibiting NMDA-receptor mediated synaptic transmission but lacking AMPA receptors) might be unsilenced (via insertion of AMPARs) to give more functional synapses [126]. Silent synapses, which are normally found at the tips of dendritic protrusions called filopodia, allow neurons to maintain more potential for plasticity and have recently been demonstrated to be more abundant in adult mice than once thought [126]. In the rTg4510 tauopathy mouse model, a loss of spine density in the cortex is reported over time and this results from a reduction in mushroom spines. However, in contrast, filopodia are increased [36, 124], suggesting that tau pathology could alter the number of silent synapses and this could contribute to changes in plasticity. In future studies, it would be interesting to examine the ratios of GLUR1/GLUR2 and also to look at AMPA phosphorylation as phosphorylation of GluA1 at serine 831 and 845 are reported to play key roles in synaptic plasticity [2].

Alteration to the generation and maintenance of theta oscillations

Functional theta oscillations are dependent upon synchronised activity within the hippocampus, which in turn is mediated by pyramidal cells and interneurons [52]. Parvalbumin (PV)-expressing interneurons are suggested to be particularly critical in regulating pyramidal cell activity [5, 102, 127].

In this study, we have demonstrated that incubation of brain slices with CSF-tau markedly enhanced theta oscillations and increased excitatory pyramidal neuron excitability, and that both of these effects were abolished upon immunodepleting for tau. It is currently unclear whether the increase in excitability of pyramidal cells and changes in glutamatergic transmission are sufficient to produce the observed increases in theta power or whether changes in GABAergic inhibition also occurred. Our findings align with existing data in rodent models and AD patients; the deposition of tau in pyramidal cells and PV interneurons from 1 month of age in 3xTg mice was associated with elevated theta oscillations but no behavioural impairments [91]. The implication that network alterations occur early in the disease course is supported by the oscillatory slowing (an increased power in the theta band) observed in early AD patients accompanied

by neuronal hypersynchronisation. Neuronal loss and a global discoordination of network activity then follows in later stages, alongside power alterations in other oscillatory bands such as alpha and delta [23, 43, 44, 54, 55, 78, 98, 99, 104, 109, 118, 119].

This leads to the question of what incubation with CSF-tau in this study might be doing to hippocampal neurons to mediate the elevation in the power of theta oscillations. A combination of experimental and simulated data has indicated that the early-stage AD hyperactivity underpinning oscillatory slowing could be due to pyramidal neuron hyperexcitability [25, 27, 49, 97, 117, 138] and/or reduced excitability of GABAergic PV interneurons and thus pyramidal cell disinhibition [4, 31, 59, 89, 97, 103, 121]. Support for the latter hypothesis of disinhibition also comes from the loss of inhibitory synapses in AD along with the pronounced GABAergic dysfunction observed in AD mouse models, including the model of APOE4, the principal genetic disease risk factor [24, 97]. Such findings provide a potential mechanism for the oscillatory disruption induced by CSF-tau incubation in this study and imply such network alterations to represent an element of the core, initial neuropathology of AD. Indeed, recent studies are now evaluating the therapeutic implementation of theta entrainment for AD patients [40, 84, 133, 134].

It has also been demonstrated that changes to theta oscillatory power—similar to what we observed herein—can be used to distinguish between prodromal AD and non-AD cases with cognitive decline [97]. The fact that our effects on oscillations agree with clinical human electrophysiological studies gives confidence that this is a method that could, in the future, be clinically useful in compliment to EEG testing.

Taking all of these changes together, it would be helpful to know whether the changes in membrane potential (4 mV depolarisation), increase in input resistance (~1/3) and reduction in rheobase are sufficient to account for the increases in the other parameters measured (e.g., baseline synaptic strength, PPF, LTP and theta oscillations). This question is difficult to answer without several additional experiments. In this proof of principle study, we only recorded from CA1 pyramidal cells. Thus, we do not know if similar effects on excitability also occur with CA3 pyramidal cells and with inhibitory interneurons. With this additional information it would be possible to construct computational models and for example determine whether these changes could account for the increase in theta oscillations and this will be explored further in future studies.

Conclusion

In this study, we have demonstrated that incubation of acutely-isolated wild-type mouse hippocampal brain slices with small volumes of diluted human CSF-tau allowed us to evaluate effects on neuronal function from single cells through to network level effects. Comparison of the toxicity profiles of the same CSF samples, with and without immuno-depletion for tau, enabled a pioneering demonstration that CSF-tau potently modulates neuronal function. We demonstrate that CSF-tau mediates an increase in neuronal excitability in single cells. We observed, at the network level, increased input–output responses and enhanced paired-pulse facilitation as well as an increase in long-term potentiation. Finally, we show that CSF-tau modifies the generation and maintenance of hippocampal theta oscillations, which have important roles in learning and memory and are known to be altered in AD patients. Together, we describe a novel method for screening human CSF to understand functional effects on neuron and network activity, which could have far-reaching benefits in understanding pathological mechanisms of tauopathies, thus allowing the development of better targeted treatments.

Supplementary Information

The online version contains supplementary material available at <https://doi.org/10.1186/s40478-023-01562-5>.

Additional file 1. Figure 1. Dose response for the effect of CSF-tau on neuronal function. Figure 2. Protocol for analysis of hippocampal CA3 theta oscillations. Figure 3. Validation of tau effects using CSF-mock-depleted.

Acknowledgements

We would like to thank Professor Bruno Freguelli for providing an interface chamber for the recording of theta oscillations.

Author contributions

Conceptualization: EH, MJW, TTK, JB, Methodology: EH, MJW, TTK, JB, Formal analysis, and Investigation: EH, MJW, JB, EC, JLR, MO, AW, BM, Writing—original draft preparation: EH, Writing—review and editing: EH, MJW, TTK, JB, EC, JLR, MO, AW, BM, HZ, KB, Resources: EH, MJW, TTK, EC, JLR, MO, HZ, KB, Supervision: EH, MJW, TTK.

Funding

EH holds a Race Against Dementia Fellowship funded by the Barbara Naylor Foundation, in collaboration with ARUK. JB is funded by the Medical Research Council doctoral training partnership at The University of Manchester. AW is funded by the Medical Research Council doctoral training partnership at the University of Warwick. TTK is funded by the Swedish Research Council (Vetenskapsrådet #2021-03244), the Alzheimer's Association Research Fellowship (#AARF-21-850325), the Aina (Ann) Wallströms and Mary-Ann Sjöbloms stiftelsen, and the Emil och Wera Cornells stiftelsen. HZ is a Wallenberg Scholar supported by grants from the Swedish Research Council (#2022-01018), the European Union's Horizon Europe research and innovation programme under grant agreement No 101053962, Swedish State Support for Clinical Research (#ALFGBG-71320), the Alzheimer Drug Discovery Foundation (ADDF), USA (#201809-2016862), the AD Strategic Fund and the Alzheimer's Association (#ADSF-21-831376-C, #ADSF-21-831381-C, and #ADSF-21-831377-C), the Bluefield Project, the Olav Thon Foundation, the Erling-Persson Family Foundation, Stiftelsen för Gamla Tjänarinnor, Hjärnfonden, Sweden (#FO2022-0270), the European Union's Horizon 2020 research and innovation programme

under the Marie Skłodowska-Curie grant agreement No 860197 (MIRIADe), the European Union Joint Programme—Neurodegenerative Disease Research (JPND2021-00694), and the UK Dementia Research Institute at UCL (UKDRI-1003). KB is supported by the Swedish Research Council (#2017-00915 and #2022-00732), the Swedish Alzheimer Foundation (#AF-930351, #AF-939721 and #AF-968270), Hjärfonden, Sweden (#FO2017-0243 and #ALZ2022-0006), the Swedish state under the agreement between the Swedish government and the County Councils, the ALF-agreement (#ALFGBG-715986 and #ALFGBG-965240), the European Union Joint Program for Neurodegenerative Disorders (JPND2019-466-236), the Alzheimer's Association 2021 Zenith Award (ZEN-21-848495), and the Alzheimer's Association 2022-2025 Grant (SG-23-1038904 QC).

Availability of data and materials

The raw data generated and analysed for this manuscript are available from the corresponding author upon reasonable request.

Declarations

Ethics approval and consent to participate

CSF collection and processing were performed at the University of Gothenburg, Sweden, with local ethical approval, and the samples sent to the University of Warwick, UK, where all experiments were done as approved by the local Human Tissue Authority and Biomedical & Scientific Research Ethics Committees. All animal care and experimental procedures were reviewed and approved by the institutional animal welfare and ethical review body (AWERB) at the University of Warwick.

Consent for publication

All authors have approved the manuscript for submission and that the contents have not been published or submitted elsewhere.

Competing interests

The authors have no conflicts of interest to declare.

Author details

¹School of Life Sciences, University of Warwick, Coventry CV4 7AL, UK. ²Division of Pharmacy and Optometry, School of Health Sciences, Faculty of Biology, Medicine and Health, University of Manchester, Manchester M13 9PL, UK. ³Department of Psychiatry and Neurochemistry, Institute of Neuroscience and Physiology, University of Gothenburg, 43180 Mölndal, Sweden. ⁴Clinical Neurochemistry Laboratory, Sahlgrenska University Hospital, 43180 Mölndal, Sweden. ⁵Department of Psychiatry, School of Medicine, University of Pittsburgh, Pittsburgh, PA 15213, USA. ⁶UK Dementia Research Institute at UCL, London WC1E 6BT, UK. ⁷Department of Neurodegenerative Disease, UCL Institute of Neurology, London WC1E 6BT, UK. ⁸Hong Kong Center for Neurodegenerative Diseases, Clear Water Bay, Hong Kong, China. ⁹Wisconsin Alzheimer's Disease Research Center, University of Wisconsin, Madison, WI 53792, USA. ¹⁰School of Medicine and Public Health, University of Wisconsin-Madison, Madison, WI 53792, USA.

Received: 14 February 2023 Accepted: 3 April 2023

Published online: 24 April 2023

References

- Acquarone E, Argyrousi EK, van den Berg M, Gulisano W, Fà M, Stanisze-wski A, Calcagno E, Zuccarello E, D'Adamio L, Deng S-X, Puzzo D, Arancio O, Fiorito J (2019) Synaptic and memory dysfunction induced by tau oligomers is rescued by up-regulation of the nitric oxide cascade. *Mol Neurodegener* 14:26. <https://doi.org/10.1186/s13024-019-0326-4>
- Ai H, Yang W, Ye M, Lu W, Yao L, Luo J (2011) Differential regulation of AMPA receptor GluA1 phosphorylation at serine 831 and 845 associated with activation of NMDA receptor subpopulations. *Neurosci Lett* 497:94–98. <https://doi.org/10.1016/j.neulet.2011.04.038>
- Akay M, Wang K, Akay Y, Dragomir A, Wu J (2009) Nonlinear dynamical analysis of carbachol induced hippocampal oscillations in mice. *Acta Pharmacol Sin*
- Ambrad Giovannetti E, Fuhrmann M (2019) Unsupervised excitation: GABAergic dysfunctions in Alzheimer's disease. *Brain Res* 1707:216–226. <https://doi.org/10.1016/j.brainres.2018.11.042>
- Amilhon B, Huh CYL, Manseau F, Ducharme G, Nichol H, Adamantidis A, Williams S (2015) Parvalbumin interneurons of hippocampus tune population activity at theta frequency. *Neuron* 86:1277–1289. <https://doi.org/10.1016/j.neuron.2015.05.027>
- Andorfer C, Kress Y, Espinoza M, de Silva R, Tucker KL, Barde Y-A, Duff K, Davies P (2003) Hyperphosphorylation and aggregation of tau in mice expressing normal human tau isoforms. *J Neurochem* 86:582–590. <https://doi.org/10.1046/j.1471-4159.2003.01879.x>
- Apartis E, Poindessous-Jazat FR, Lamour YA, Bassant MH (1998) Loss of rhythmically bursting neurons in rat medial septum following selective lesion of septohippocampal cholinergic system. *J Neurophysiol* 79:1633–1642. <https://doi.org/10.1152/jn.1998.79.4.1633>
- Ashton NJ, Pascoal TA, Karikari TK, Benedet AL, Lantero-Rodriguez J, Brinkmalm G, Snellman A, Schöll M, Troakes C, Hye A, Gauthier S, Vanmechelen E, Zetterberg H, Rosa-Neto P, Blennow K (2021) Plasma p-tau231: a new biomarker for incipient Alzheimer's disease pathology. *Acta Neuropathol (Berl)* 141:709–724. <https://doi.org/10.1007/s00401-021-02275-6>
- Auger C, Marty A (2000) Quantal currents at single-site central synapses. *J Physiol* 526:3–11. <https://doi.org/10.1111/j.1469-7793.2000.t013-00003.x>
- Badel L, Lefort S, Berger TK, Petersen CCH, Gerstner W, Richardson MJE (2008) Extracting non-linear integrate-and-fire models from experimental data using dynamic I-V curves. *Biol Cybern* 99:361–370. <https://doi.org/10.1007/s00422-008-0259-4>
- Badel L, Lefort S, Brette R, Petersen CCH, Gerstner W, Richardson MJE (2008) Dynamic I-V curves are reliable predictors of naturalistic pyramidal-neuron voltage traces. *J Neurophysiol* 99:656–666. <https://doi.org/10.1152/jn.01107.2007>
- Bassett SS, Yousem DM, Cristinzio C, Kusevic I, Yassa MA, Caffo BS, Zeger SL (2006) Familial risk for Alzheimer's disease alters fMRI activation patterns. *Brain J Neurol* 129:1229–1239. <https://doi.org/10.1093/brain/awl089>
- Begus K, Bonawitz E (2020) The rhythm of learning: Theta oscillations as an index of active learning in infancy. *Dev Cogn Neurosci* 45:100810. <https://doi.org/10.1016/j.dcn.2020.100810>
- Bennys K, Rondouin G, Vergnes C, Touchon J (2001) Diagnostic value of quantitative EEG in Alzheimer's disease. *Neurophysiol Clin Neurophysiol* 31:153–160. [https://doi.org/10.1016/S0987-7053\(01\)00254-4](https://doi.org/10.1016/S0987-7053(01)00254-4)
- Berry SD, Thompson RF (1978) Prediction of learning rate from the hippocampal electroencephalogram. *Science* 200:1298–1300. <https://doi.org/10.1126/science.663612>
- Bezanson J, Edelman A, Karpinski S, Shah VB (2017) Julia: a fresh approach to numerical computing. *SIAM Rev* 59:65–98. <https://doi.org/10.1137/141000671>
- Bjorefeldt A, Andreasson U, Daborg J, Riebe I, Wasling P, Zetterberg H, Hanse E (2015) Human cerebrospinal fluid increases the excitability of pyramidal neurons in the in vitro brain slice. *J Physiol* 593:231–243. <https://doi.org/10.1113/jphysiol.2014.284711>
- Blennow K, Chen C, Cicognola C, Wildsmith KR, Manser PT, Bohorquez SMS, Zhang Z, Xie B, Peng J, Hansson O, Kvartsberg H, Portelius E, Zetterberg H, Lashley T, Brinkmalm G, Kerchner GA, Weimer RM, Ye K, Höglund K (2020) Cerebrospinal fluid tau fragment correlates with tau PET: a candidate biomarker for tangle pathology. *Brain* 143:650–660. <https://doi.org/10.1093/brain/awz346>
- Blennow K, Zetterberg H (2018) Biomarkers for Alzheimer's disease: current status and prospects for the future. *J Intern Med* 284:643–663. <https://doi.org/10.1111/joim.12816>
- Booth CA, Witton J, Nowacki J, Tsaneva-Atanasova K, Jones MW, Randall AD, Brown JT (2016) Altered intrinsic pyramidal neuron properties and pathway-specific synaptic dysfunction underlie aberrant hippocampal network function in a mouse model of tauopathy. *J Neurosci* 36:350–363. <https://doi.org/10.1523/JNEUROSCI.2151-15.2016>
- Braak H, Braak E (1991) Neuropathological staging of Alzheimer-related changes. *Acta Neuropathol (Berl)* 82:239–259. <https://doi.org/10.1007/BF00308809>
- Brzezicka A, Kamiński J, Reed CM, Chung JM, Mamelak AN, Rutishauser U (2019) Working memory load-related theta power decreases in

- dorsolateral prefrontal cortex predict individual differences in performance. *J Cogn Neurosci* 31:1290–1307. https://doi.org/10.1162/jocn_a_01417
23. Busche MA (2019) Tau suppresses neuronal activity in vivo, even before tangles form. *Brain J Neurol* 142:843–846. <https://doi.org/10.1093/brain/awz060>
 24. Busche MA, Eichhoff G, Adelsberger H, Abramowski D, Wiederhold K-H, Haass C, Staufenbiel M, Konnerth A, Garaschuk O (2008) Clusters of hyperactive neurons near amyloid plaques in a mouse model of Alzheimer's disease. *Science* 321:1686–1689. <https://doi.org/10.1126/science.1162844>
 25. Busche MA, Konnerth A (2015) Neuronal hyperactivity—A key defect in Alzheimer's disease? *BioEssays News Rev Mol Cell Dev Biol* 37:624–632. <https://doi.org/10.1002/bies.201500004>
 26. Bush D, Bisby JA, Bird CM, Gollwitzer S, Rodionov R, Diehl B, McEvoy AW, Walker MC, Burgess N (2017) Human hippocampal theta power indicates movement onset and distance travelled. *Proc Natl Acad Sci U S A* 114:12297–12302. <https://doi.org/10.1073/pnas.1708716114>
 27. Cardin JA, Carlén M, Meletis K, Knoblich U, Zhang F, Deisseroth K, Tsai L-H, Moore CI (2009) Driving fast-spiking cells induces gamma rhythm and controls sensory responses. *Nature* 459:663–667. <https://doi.org/10.1038/nature08002>
 28. Celone KA, Calhoun VD, Dickerson BC, Atri A, Chua EF, Miller SL, DePeau K, Rentz DM, Selkoe DJ, Blacker D, Albert MS, Sperling RA (2006) Alterations in memory networks in mild cognitive impairment and Alzheimer's disease: an independent component analysis. *J Neurosci Off J Soc Neurosci* 26:10222–10231. <https://doi.org/10.1523/JNEUROSCI.2250-06.2006>
 29. Chen Z, Mengel D, Keshavan A, Rissman RA, Billinton A, Perkinson M, Percival-Alwyn J, Schultz A, Properzi M, Johnson K, Selkoe DJ, Sperling RA, Patel P, Zetterberg H, Galasko D, Schott JM, Walsh DM (2019) Learnings about the complexity of extracellular tau aid development of a blood-based screen for Alzheimer's disease. *Alzheimers Dement J Alzheimers Assoc* 15:487–496. <https://doi.org/10.1016/j.jalz.2018.09.010>
 30. Chung DC, Roemer S, Petrucelli L, Dickson DW (2021) Cellular and pathological heterogeneity of primary tauopathies. *Mol Neurodegener* 16:57. <https://doi.org/10.1186/s13024-021-00476-x>
 31. Chung H, Park K, Jang HJ, Kohl MM, Kwag J (2020) Dissociation of somatostatin and parvalbumin interneurons circuit dysfunctions underlying hippocampal theta and gamma oscillations impaired by amyloid β oligomers in vivo. *Brain Struct Funct* 225:935–954. <https://doi.org/10.1007/s00429-020-02044-3>
 32. Cicognola C, Brinkmalm G, Wahlgren J, Portelius E, Gobom J, Cullen NC, Hansson O, Parnetti L, Constantinescu R, Wildsmith K, Chen H-H, Beach TG, Lashley T, Zetterberg H, Blennow K, Höglund K (2019) Novel tau fragments in cerebrospinal fluid: relation to tangle pathology and cognitive decline in Alzheimer's disease. *Acta Neuropathol (Berl)* 137:279–296. <https://doi.org/10.1007/s00401-018-1948-2>
 33. Coben LA, Chi D, Snyder AZ, Storandt M (1990) Replication of a study of frequency analysis of the resting awake EEG in mild probable Alzheimer's disease. *Electroencephalogr Clin Neurophysiol* 75:148–154. [https://doi.org/10.1016/0013-4694\(90\)90168-j](https://doi.org/10.1016/0013-4694(90)90168-j)
 34. Cowan CM, Chee F, Shepherd D, Mudher A (2010) Disruption of neuronal function by soluble hyperphosphorylated tau in a *Drosophila* model of tauopathy. *Biochem Soc Trans* 38:564–570. <https://doi.org/10.1042/BST0380564>
 35. Crespo-García M, Zeiller M, Leupold C, Kreiselmeyer G, Rampp S, Hamer HM, Dalal SS (2016) Slow-theta power decreases during item-place encoding predict spatial accuracy of subsequent context recall. *Neuroimage* 142:533
 36. Crimins JL, Rocher AB, Peters A, Shultz P, Lewis J, Luebke JI (2011) Homeostatic responses by surviving cortical pyramidal cells in neurodegenerative tauopathy. *Acta Neuropathol (Berl)* 122:551–564. <https://doi.org/10.1007/s00401-011-0877-0>
 37. Czigler B, Csikós D, Hidasi Z, Anna Gaál Z, Csibri E, Kiss E, Salacz P, Molnár M (2008) Quantitative EEG in early Alzheimer's disease patients - power spectrum and complexity features. *Int J Psychophysiol Off J Int Organ Psychophysiol* 68:75–80. <https://doi.org/10.1016/j.ijpsycho.2007.11.002>
 38. DaSilva LLP, Wall MJ, de Almeida L, Wauters SC, Januário YC, Müller J, Corrêa SAL (2016) Activity-regulated cytoskeleton-associated protein controls ampar endocytosis through a direct interaction with clathrin-adaptor protein 2. *eNeuro*. <https://doi.org/10.1523/ENEURO.0144-15.2016>
 39. Datta D, Leslie SN, Wang M, Morozov YM, Yang S, Mentone S, Zeiss C, Duque A, Rakic P, Horvath TL, van Dyck CH, Nairn AC, Arnsten AFT (2021) Age-related calcium dysregulation linked with tau pathology and impaired cognition in non-human primates. *Alzheimers Dement* 17:920–932. <https://doi.org/10.1002/alz.12325>
 40. Di Lorenzo F, Bonni S, Picazio S, Motta C, Caltagirone C, Martorana A, Koch G (2020) Effects of cerebellar theta burst stimulation on contralateral motor cortex excitability in patients with Alzheimer's disease. *Brain Topogr* 33:613–617. <https://doi.org/10.1007/s10548-020-00781-6>
 41. Dickerson BC, Salat DH, Greve DN, Chua EF, Rand-Giovannetti E, Rentz DM, Bertram L, Mullin K, Tanzi RE, Blacker D, Albert MS, Sperling RA (2005) Increased hippocampal activation in mild cognitive impairment compared to normal aging and AD. *Neurology* 65:404–411. <https://doi.org/10.1212/01.wnl.0000171450.97464.49>
 42. Ekstrom AD, Caplan JB, Ho E, Shattuck K, Fried I, Kahana MJ (2005) Human hippocampal theta activity during virtual navigation. *Hippocampus* 15:881–889. <https://doi.org/10.1002/hipo.20109>
 43. Engels MMA, van der Flier WM, Stam CJ, Hillebrand A, Scheltens P, van Straaten ECW (2017) Alzheimer's disease: The state of the art in resting-state magnetoencephalography. *Clin Neurophysiol Off J Int Fed Clin Neurophysiol* 128:1426–1437. <https://doi.org/10.1016/j.clinph.2017.05.012>
 44. Engels MMA, Hillebrand A, van der Flier WM, Stam CJ, Scheltens P, van Straaten ECW (2016) Slowing of hippocampal activity correlates with cognitive decline in early onset Alzheimer's disease. An MEG study with virtual electrodes. *Front Hum Neurosci* 10:238. <https://doi.org/10.3389/fnhum.2016.00238>
 45. Fáb M, Puzzo D, Piacentini R, Staniszewski A, Zhang H, Baltrons MA, Li Puma DD, Chatterjee I, Li J, Saeed F, Berman HL, Ripoli C, Gulisano W, Gonzalez J, Tian H, Costa JA, Lopez P, Davidowitz E, Yu WH, Haroutunian V, Brown LM, Palmeri A, Sigurdsson EM, Duff KE, Teich AF, Honig LS, Sierks M, Moe JG, D'Adamio L, Grassi C, Kanaan NM, Fraser PE, Arancio O (2016) Extracellular tau oligomers produce an immediate impairment of LTP and memory. *Sci Rep* 6:19393. <https://doi.org/10.1038/srep19393>
 46. Fellous J-M, Sejnowski TJ (2000) Cholinergic induction of oscillations in the hippocampal slice in the slow (0.5–2 Hz), theta (5–12 Hz), and gamma (35–70 Hz) bands. *Hippocampus* 10:187–197. [https://doi.org/10.1002/\(SICI\)1098-1063\(2000\)10:2%3c187::AID-HIPO8%3e3.0.CO;2-M](https://doi.org/10.1002/(SICI)1098-1063(2000)10:2%3c187::AID-HIPO8%3e3.0.CO;2-M)
 47. Fernández A, Maestú F, Amo C, Gil P, Fehr T, Wienbruch C, Rockstroh B, Elbert T, Ortiz T (2002) Focal temporoparietal slow activity in Alzheimer's disease revealed by magnetoencephalography. *Biol Psychiatry* 52:764–770. [https://doi.org/10.1016/S0006-3223\(02\)01366-5](https://doi.org/10.1016/S0006-3223(02)01366-5)
 48. Filippini N, MacIntosh BJ, Hough MG, Goodwin GM, Frisoni GB, Smith SM, Matthews PM, Beckmann CF, Mackay CE (2009) Distinct patterns of brain activity in young carriers of the APOE-epsilon4 allele. *Proc Natl Acad Sci U S A* 106:7209–7214. <https://doi.org/10.1073/pnas.0811879106>
 49. Ghatak S, Dolatabadi N, Trudler D, Zhang X, Wu Y, Mohata M, Ambasadhan R, Talantova M, Lipton SA (2019) Mechanisms of hyperexcitability in Alzheimer's disease hiPSC-derived neurons and cerebral organoids vs isogenic controls. *Elife* 8:e50333. <https://doi.org/10.7554/eLife.50333>
 50. Gobom J, Benedet AL, Mattsson-Carlgrén N, Montoliu-Gaya L, Schultz N, Ashton NJ, Janelidze S, Servaes S, Sauer M, Pascoal TA, Karikari TK, Lantero-Rodriguez J, Brinkmalm G, Zetterberg H, Hansson O, Rosa-Neto P, Blennow K (2022) Antibody-free measurement of cerebrospinal fluid tau phosphorylation across the Alzheimer's disease continuum. *Mol Neurodegener* 17:81. <https://doi.org/10.1186/s13024-022-00586-0>
 51. Gobom J, Parnetti L, Rosa-Neto P, Vyhnaček M, Gauthier S, Cataldi S, Lerch O, Lacco J, Cechova K, Clarin M, Benet AL, Pascoal TA, Rahmouni N, Vandijck M, Huyck E, Bastard NL, Stevenson J, Chamoun M, Alcolea D, Lleó A, Andreasson U, Verbeek MM, Bellomo G, Rinaldi R, Ashton NJ, Zetterberg H, Sheardova K, Hort J, Blennow K (2022) Validation of the LUMIPULSE automated immunoassay for the measurement of core AD biomarkers in cerebrospinal fluid. *Clin Chem Lab Med CCLM* 60:207–219. <https://doi.org/10.1515/cclm-2021-0651>
 52. Goutagny R, Jackson J, Williams S (2009) Self-generated theta oscillations in the hippocampus. *Nat Neurosci* 12:1491–1493. <https://doi.org/10.1038/nn.2440>

53. Goutagny R, Krantic S (2013) Hippocampal oscillatory activity in Alzheimer's disease: toward the identification of early biomarkers? *Aging Dis* 4:134–140
54. de Haan W, Mott K, van Straaten ECW, Scheltens P, Stam CJ (2012) Activity dependent degeneration explains hub vulnerability in Alzheimer's disease. *PLoS Comput Biol* 8:1002582. <https://doi.org/10.1371/journal.pcbi.1002582>
55. de Haan W, Stam CJ, Jones BF, Zuiderwijk IM, van Dijk BW, Scheltens P (2008) Resting-state oscillatory brain dynamics in Alzheimer disease. *J Clin Neurophysiol Off Publ Am Electroencephalogr Soc* 25:187–193. <https://doi.org/10.1097/WNP.0b013e31817da184>
56. Hämäläinen A, Pihlajamäki M, Tanila H, Hänninen T, Niskanen E, Tervo S, Karjalainen PA, Vanninen RL, Soininen H (2007) Increased fMRI responses during encoding in mild cognitive impairment. *Neurobiol Aging* 28:1889–1903. <https://doi.org/10.1016/j.neurobiolaging.2006.08.008>
57. Han P, Serrano G, Beach TG, Caselli RJ, Yin J, Zhuang N, Shi J (2017) A quantitative analysis of brain soluble tau and the tau secretion factor. *J Neuropathol Exp Neurol* 76:44–51. <https://doi.org/10.1093/jnen/nlw105>
58. Harrison PM, Badel L, Wall MJ, Richardson MJE (2015) Experimentally verified parameter sets for modelling heterogeneous neocortical pyramidal-cell populations. *PLoS Comput Biol* 11:e1004165. <https://doi.org/10.1371/journal.pcbi.1004165>
59. Hijazi S, Heistek TS, Scheltens P, Neumann U, Shimshek DR, Mansvelder HD, Smit AB, van Kesteren RE (2020) Early restoration of parvalbumin interneuron activity prevents memory loss and network hyperexcitability in a mouse model of Alzheimer's disease. *Mol Psychiatry* 25:3380–3398. <https://doi.org/10.1038/s41380-019-0483-4>
60. Hill E, Karikari TK, Lantero-Rodriguez J, Zetterberg H, Blennow K, Richardson MJ, Wall MJ (2021) Truncating tau reveals different pathophysiological actions of oligomers in single neurons. *Commun Biol* 4:1265. <https://doi.org/10.1038/s42003-021-02791-x>
61. Hill E, Karikari TK, Moffat KG, Richardson MJE, Wall MJ (2019) Introduction of tau oligomers into cortical neurons alters action potential dynamics and disrupts synaptic transmission and plasticity. *Eneuro* 6:ENEURO.0166-19.2019. <https://doi.org/10.1523/ENEURO.0166-19.2019>
62. Hill E, Wall MJ, Moffat KG, Karikari TK (2020) Understanding the pathophysiological actions of tau oligomers: a critical review of current electrophysiological approaches. *Front Mol Neurosci*. <https://doi.org/10.3389/fnmol.2020.00155>
63. Hölscher C, McGlinchey L, Anwyl R, Rowan MJ (1997) HFS-induced long-term potentiation and LFS-induced depotentiation in area CA1 of the hippocampus are not good models for learning. *Psychopharmacology* 130:174–182. <https://doi.org/10.1007/s002130050226>
64. Horie K, Barthélemy NR, Sato C, Bateman RJ (2020) CSF tau microtubule binding region identifies tau tangle and clinical stages of Alzheimer's disease. *Brain* 144:515–527. <https://doi.org/10.1093/brain/awaa373>
65. Horie K, Barthélemy NR, Spina S, VandeVrede L, He Y, Paterson RW, Wright BA, Day GS, Davis AA, Karch CM, Seeley WW, Perrin RJ, Kopisetti RK, Shaikh F, Lago AL, Heuer HW, Ghoshal N, Gabelle A, Miller BL, Boxer AL, Bateman RJ, Sato C (2022) CSF tau microtubule-binding region identifies pathological changes in primary tauopathies. *Nat Med* 28:2547–2554. <https://doi.org/10.1038/s41591-022-02075-9>
66. Hsiao F-J, Wang Y-J, Yan S-H, Chen W-T, Lin Y-Y (2013) Altered oscillation and synchronization of default-mode network activity in mild Alzheimer's disease compared to mild cognitive impairment: an electrophysiological study. *PLoS ONE* 8:e68792. <https://doi.org/10.1371/journal.pone.0068792>
67. Ishida K, Yamada K, Nishiyama R, Hashimoto T, Nishida I, Abe Y, Yasui M, Iwatsubo T (2022) Glymphatic system clears extracellular tau and protects from tau aggregation and neurodegeneration. *J Exp Med* 219:e10211275. <https://doi.org/10.1084/jem.20211275>
68. Ishikawa T, Sahara Y, Takahashi T (2002) A single packet of transmitter does not saturate postsynaptic glutamate receptors. *Neuron* 34:613–621. [https://doi.org/10.1016/S0896-6273\(02\)00692-X](https://doi.org/10.1016/S0896-6273(02)00692-X)
69. Jack CR, Bennett DA, Blennow K, Carrillo MC, Dunn B, Haeberlein SB, Holtzman DM, Jagust W, Jessen F, Karlawish J, Liu E, Molinuevo JL, Montine T, Phelps C, Rankin KP, Rowe CC, Scheltens P, Siemers E, Snyder HM, Sperling R, Contributors, (2018) NIA-AA Research Framework: Toward a biological definition of Alzheimer's disease. *Alzheimers Dement J Alzheimers Assoc* 14:535–562. <https://doi.org/10.1016/j.jalz.2018.02.018>
70. Jelic V, Johansson SE, Almkvist O, Shigeta M, Julin P, Nordberg A, Winblad B, Wahlund LO (2000) Quantitative electroencephalography in mild cognitive impairment: longitudinal changes and possible prediction of Alzheimer's disease. *Neurobiol Aging* 21:533–540. [https://doi.org/10.1016/s0197-4580\(00\)00153-6](https://doi.org/10.1016/s0197-4580(00)00153-6)
71. Jeong J (2004) EEG dynamics in patients with Alzheimer's disease. *Clin Neurophysiol Off J Int Fed Clin Neurophysiol* 115:1490–1505. <https://doi.org/10.1016/j.clinph.2004.01.001>
72. Jin Y, Su Q-X, Shen J-X, Marks MJ, Wu J (2013) Impaired hippocampal theta oscillations in the mice null alpha7 nicotinic acetylcholine receptors. *CNS Neurosci Ther* 19:721–723. <https://doi.org/10.1111/cns.12138>
73. Kanmert D, Cantlon A, Muratore CR, Jin M, O'Malley TT, Lee G, Young-Pearse TL, Selkoe DJ, Walsh DM (2015) C-terminally truncated forms of tau, but not full-length tau or its c-terminal fragments, are released from neurons independently of cell death. *J Neurosci* 35:10851–10865. <https://doi.org/10.1523/JNEUROSCI.0387-15.2015>
74. Karikari TK, Ashton NJ, Brinkmalm G, Brum WS, Benedet AL, Montoliu-Gaya L, Lantero-Rodriguez J, Pascoal TA, Suárez-Calvet M, Rosa-Neto P, Blennow K, Zetterberg H (2022) Blood phospho-tau in Alzheimer disease: analysis, interpretation, and clinical utility. *Nat Rev Neurol* 18:400–418. <https://doi.org/10.1038/s41582-022-00665-2>
75. Karikari TK, Benedet AL, Ashton NJ, Lantero-Rodriguez J, Snellman A, Suárez-Calvet M, Saha-Chaudhuri P, Lussier F, Kvartsberg H, Rial AM, Pascoal TA, Andreasson U, Schöll M, Weiner MW, Rosa-Neto P, Trojanowski JQ, Shaw LM, Blennow K, Zetterberg H (2021) Alzheimer's Disease Neuroimaging Initiative. Diagnostic performance and prediction of clinical progression of plasma phospho-tau181 in the Alzheimer's Disease Neuroimaging Initiative. *Mol Psychiatry* 26:429–442. <https://doi.org/10.1038/s41380-020-00923-z>
76. Karikari TK, Pascoal TA, Ashton NJ, Janelidze S, Benedet AL, Rodriguez JL, Chamoun M, Savard M, Kang MS, Theriault J, Schöll M, Massarweh G, Soucy J-P, Höglund K, Brinkmalm G, Mattsson N, Palmqvist S, Gauthier S, Stomrud E, Zetterberg H, Hansson O, Rosa-Neto P, Blennow K (2020) Blood phosphorylated tau 181 as a biomarker for Alzheimer's disease: a diagnostic performance and prediction modelling study using data from four prospective cohorts. *Lancet Neurol* 19:422–433. [https://doi.org/10.1016/S1474-4422\(20\)30071-5](https://doi.org/10.1016/S1474-4422(20)30071-5)
77. Kim S-P, Kang J-H, Choe S-H, Jeong JW, Kim HT, Yun K, Jeong J, Lee S-H (2012) Modulation of theta phase synchronization in the human electroencephalogram during a recognition memory task. *NeuroReport* 23:637–641. <https://doi.org/10.1097/WNR.0b013e318238354afed>
78. Koelewijn L, Lancaster TM, Linden D, Dima DC, Routley BC, Magazzini L, Barawi K, Brindley L, Adams R, Tansey KE, Bompas A, Tales A, Bayer A, Singh K (2019) Oscillatory hyperactivity and hyperconnectivity in young APOE-ε4 carriers and hypoconnectivity in Alzheimer's disease. *Elife* 8:e36011. <https://doi.org/10.7554/eLife.36011>
79. Lantero-Rodriguez J, Snellman A, Benedet AL, Milà-Alomà M, Camporesi E, Montoliu-Gaya L, Ashton NJ, Vrillon A, Karikari TK, Gispert JD, Salvadó G, Shekari M, Toomey CE, Lashley TL, Zetterberg H, Suárez-Calvet M, Brinkmalm G, Rosa Neto P, Blennow K (2021) P-tau235: a novel biomarker for staging preclinical Alzheimer's disease. *EMBO Mol Med* 13:e15098. <https://doi.org/10.15252/emmm.202115098>
80. Lasagna-Reeves CA, Castillo-Carranza DL, Sengupta U, Guerrero-Munoz MJ, Kiritoshi T, Neugebauer V, Jackson GR, Kaye R (2012) Alzheimer brain-derived tau oligomers propagate pathology from endogenous tau. *Sci Rep* 2:700. <https://doi.org/10.1038/srep00700>
81. Lasagna-Reeves CA, Castillo-Carranza DL, Sengupta U, Sarmiento J, Troncoso J, Jackson GR, Kaye R (2012) Identification of oligomers at early stages of tau aggregation in Alzheimer's disease. *FASEB J Off Publ Fed Am Soc Exp Biol* 26:1946–1959. <https://doi.org/10.1096/fj.11-199851>
82. Leitão MJ, Silva-Spinola A, Santana I, Olmedo V, Nadal A, Le Bastard N, Baldeiras I (2019) Clinical validation of the Lumipulse G cerebrospinal fluid assays for routine diagnosis of Alzheimer's disease. *Alzheimers Res Ther* 11:91. <https://doi.org/10.1186/s13195-019-0550-8>
83. Leung LS, Fu XW (1994) Factors affecting paired-pulse facilitation in hippocampal CA1 neurons in vitro. *Brain Res* 650:75–84. [https://doi.org/10.1016/0006-8993\(94\)90209-7](https://doi.org/10.1016/0006-8993(94)90209-7)

84. Li G, Bien-Ly N, Andrews-Zwilling Y, Xu Q, Bernardo A, Ring K, Halabisky B, Deng C, Mahley RW, Huang Y (2009) GABAergic interneuron dysfunction impairs hippocampal neurogenesis in adult apolipoprotein E4 knockin mice. *Cell Stem Cell* 5:634–645. <https://doi.org/10.1016/j.stem.2009.10.015>
85. Lisman JE, Jensen O (2013) The θ -y neural code. *Neuron* 77:1002–1016. <https://doi.org/10.1016/j.neuron.2013.03.007>
86. Liu G, Choi S, Tsien RW (1999) Variability of neurotransmitter concentration and nonsaturation of postsynaptic AMPA receptors at synapses in hippocampal cultures and slices. *Neuron* 22:395–409. [https://doi.org/10.1016/S0896-6273\(00\)81099-5](https://doi.org/10.1016/S0896-6273(00)81099-5)
87. Luo Y, Huang L, Liao P, Jiang R (2021) Contribution of neuronal and glial two-pore-domain potassium channels in health and neurological disorders. *Neural Plast* 2021:8643129. <https://doi.org/10.1155/2021/8643129>
88. Maeda S, Sahara N, Saito Y, Murayama S, Ikai A, Takashima A (2006) Increased levels of granular tau oligomers: an early sign of brain aging and Alzheimer's disease. *Neurosci Res* 54:197–201. <https://doi.org/10.1016/j.neures.2005.11.009>
89. Martinez-Losa M, Tracy TE, Ma K, Verret L, Clemente-Perez A, Khan AS, Cobos I, Ho K, Gan L, Mucke L, Alvarez-Dolado M, Palop JJ (2018) Nav1.1-overexpressing interneuron transplants restore brain rhythms and cognition in a mouse model of Alzheimer's disease. *Neuron* 98:75–89.e5. <https://doi.org/10.1016/j.neuron.2018.02.029>
90. Meredith JE Jr, Sankaranarayanan S, Guss V, Lanzetti AJ, Berisha F, Neely RJ, Slemmon JR, Portelius E, Zetterberg H, Blennow K, Soares H, Ahlji-nian M, Albright CF (2013) Characterization of novel CSF tau and ptau biomarkers for Alzheimer's disease. *PLoS ONE* 8:e76523. <https://doi.org/10.1371/journal.pone.0076523>
91. Mondragón-Rodríguez S, Salas-Gallardo A, González-Pereyra P, Macías M, Ordaz B, Peña-Ortega F, Aguilar-Vázquez A, Orta-Salazar E, Díaz-Cintra S, Perry G, Williams S (2018) Phosphorylation of Tau protein correlates with changes in hippocampal theta oscillations and reduces hippocampal excitability in Alzheimer's model. *J Biol Chem* 293:8462–8472. <https://doi.org/10.1074/jbc.RA117.001187>
92. Moretti DV, Babiloni C, Binetti G, Cassetta E, Dal Forno G, Ferreri F, Ferri R, Lanuzza B, Miniussi C, Nobili F, Rodríguez G, Salinari S, Rossini PM (2004) Individual analysis of EEG frequency and band power in mild Alzheimer's disease. *Clin Neurophysiol* 115:299–308. [https://doi.org/10.1016/S1388-2457\(03\)00345-6](https://doi.org/10.1016/S1388-2457(03)00345-6)
93. Mormino E, Brandel M, Madison C, Marks S, Baker S, Jagust WJ (2011) A β deposition in aging is associated with increases in brain activation during successful memory encoding. *Cerebral Cortex*. Oxford Academic
94. Musæus CS, Engedal K, Høgh P, Jelic V, Mørup M, Naik M, Oeksengaard A-R, Snaedal J, Wahlund L-O, Waldemar G, Andersen BB (2018) EEG theta power is an early marker of cognitive decline in dementia due to Alzheimer's disease. *J Alzheimers Dis JAD* 64:1359–1371. <https://doi.org/10.3233/JAD-180300>
95. Nelson PT, Alafuzoff I, Bigio EH, Bouras C, Braak H, Cairns NJ, Castellani RJ, Crain BJ, Davies P, Del Tredici K, Duyckaerts C, Frosch MP, Haroutunian V, Hof PR, Hulette CM, Hyman BT, Iwatsubo T, Jellinger KA, Jicha GA, Kovari E, Kukull WA, Leverenz JB, Love S, Mackenzie IR, Mann DM, Masliah E, McKee AC, Montine TJ, Morris JC, Schneider JA, Sonnen JA, Thal DR, Trojanowski JQ, Troncoso JC, Wisniewski T, Woltjer RL, Beach TG (2012) Correlation of Alzheimer disease neuropathologic changes with cognitive status: a review of the literature. *J Neuropathol Exp Neurol* 71:362–381. <https://doi.org/10.1097/NEN.0b013e31825018f7>
96. Niewiadomska G, Niewiadomski W, Steczkowska M, Gasiorowska A (2021) Tau Oligomers. *Neurotoxicity Life* 11:28. <https://doi.org/10.3390/life11010028>
97. van Nifterick AM, Gouw AA, van Kesteren RE, Scheltens P, Stam CJ, de Haan W (2022) A multiscale brain network model links Alzheimer's disease-mediated neuronal hyperactivity to large-scale oscillatory slowing. *Alzheimers Res Ther* 14:101. <https://doi.org/10.1186/s13195-022-01041-4>
98. Ochoa JF, Alonso JF, Duque JE, Tobón CA, Baena A, Lopera F, Mañanas MA, Hernández AM (2017) Precuneus failures in subjects of the PSEN1 E280A family at risk of developing Alzheimer's disease detected using quantitative electroencephalography. *J Alzheimers Dis* 58:1229
99. Ochoa JF, Alonso JF, Duque JE, Tobón CA, Mañanas MA, Lopera F, Hernández AM (2017) Successful object encoding induces increased directed connectivity in presymptomatic early-onset Alzheimer's disease. *J Alzheimers Dis* 55:1195–1205. <https://doi.org/10.3233/JAD-160803>
100. Oertner TG, Sabatini BL, Nimchinsky EA, Svoboda K (2002) Facilitation at single synapses probed with optical quantal analysis. *Nat Neurosci* 5:657–664. <https://doi.org/10.1038/nm867>
101. Osipova D, Ahveninen J, Jensen O, Ylikoski A, Pekkonen E (2005) Altered generation of spontaneous oscillations in Alzheimer's disease. *Neuroimage* 27:835–841. <https://doi.org/10.1016/j.neuroimage.2005.05.011>
102. Palop JJ, Chin J, Roberson ED, Wang J, Thwin MT, Bien-Ly N, Yoo J, Ho KO, Yu G-Q, Kreitzer A, Finkbeiner S, Noebels JL, Mucke L (2007) Aberrant excitatory neuronal activity and compensatory remodeling of inhibitory hippocampal circuits in mouse models of Alzheimer's disease. *Neuron* 55:697–711. <https://doi.org/10.1016/j.neuron.2007.07.025>
103. Palop JJ, Mucke L (2016) Network abnormalities and interneuron dysfunction in Alzheimer disease. *Nat Rev Neurosci* 17:777–792. <https://doi.org/10.1038/nrn.2016.141>
104. Pusił S, López ME, Cuesta P, Bruña R, Pereda E, Maestú F (2019) Hyper-synchronization in mild cognitive impairment: the "X" model. *Brain J Neurol* 142:3936–3950. <https://doi.org/10.1093/brain/awz320>
105. Puzzo D, Piacentini R, Fá M, Gulisano W, Li Puma DD, Staniszewski A, Zhang H, Tropea MR, Cocco S, Palmeri A, Fraser P, D'Adamo L, Grassi C, Arancio O (2017) LTP and memory impairment caused by extracellular A β and Tau oligomers is APP-dependent. *Elife*. <https://doi.org/10.7554/eLife.26991>
106. Raghavachari S, Kahana MJ, Rizzuto DS, Caplan JB, Kirschen MP, Bourgeois B, Madsen JR, Lisman JE (2001) Gating of human theta oscillations by a working memory task. *J Neurosci Off J Soc Neurosci* 21:3175–3183. <https://doi.org/10.1523/JNEUROSCI.21-09-03175.2001>
107. Regan P, Piers T, Yi J-H, Kim D-H, Huh S, Park SJ, Ryu JH, Whitcomb DJ, Cho K (2015) Tau phosphorylation at serine 396 residue is required for hippocampal LTD. *J Neurosci Off J Soc Neurosci* 35:4804–4812. <https://doi.org/10.1523/JNEUROSCI.2842-14.2015>
108. Rocher AB, Crimins JL, Amatrudo JM, Kinson MS, Todd-Brown MA, Lewis J, Luebke JI (2010) Structural and functional changes in tau mutant mice neurons are not linked to the presence of NFTs. *Exp Neurol* 223:385–393. <https://doi.org/10.1016/j.expneurol.2009.07.029>
109. Rodríguez GA, Barrett GM, Duff KE, Hussaini SA (2020) Chemogenetic attenuation of neuronal activity in the entorhinal cortex reduces A β and tau pathology in the hippocampus. *PLoS Biol* 18:e3000851. <https://doi.org/10.1371/journal.pbio.3000851>
110. Sato C, Barthélemy NR, Mawuenyega KG, Patterson BW, Gordon BA, Jockel-Balsarotti J, Sullivan M, Crisp MJ, Kasten T, Kirmess KM, Kanaan NM, Yarasheski KE, Baker-Nigh A, Benzinger TLS, Miller TM, Karch CM, Bateman RJ (2018) Tau kinetics in neurons and the human central nervous system. *Neuron* 97:1284–1298.e7. <https://doi.org/10.1016/j.neuron.2018.02.015>
111. Scheltens P, Blennow K, Breteler MMB, de Strooper B, Frisoni GB, Sal-loway S, Van der Flier WM (2016) Alzheimer's disease. *Lancet Lond Engl* 388:505–517. [https://doi.org/10.1016/S0140-6736\(15\)01124-1](https://doi.org/10.1016/S0140-6736(15)01124-1)
112. Schreiter-Gasser U, Gasser T, Ziegler P (1994) Quantitative EEG analysis in early onset Alzheimer's disease: correlations with severity, clinical characteristics, visual EEG and CCT. *Electroencephalogr Clin Neurophysiol* 90:267–272. [https://doi.org/10.1016/0013-4694\(94\)90144-9](https://doi.org/10.1016/0013-4694(94)90144-9)
113. Serrano-Pozo A, Frosch MP, Masliah E, Hyman BT (2011) Neuropathological alterations in Alzheimer disease. *Cold Spring Harb Perspect Med* 1:a006189. <https://doi.org/10.1101/cshperspect.a006189>
114. Setti SE, Hunsberger HC, Reed MN (2017) Alterations in hippocampal activity and Alzheimer's disease. *Transl Issues Psychol Sci* 3:348–356. <https://doi.org/10.1037/tps0000124>
115. Shafiei SS, Guerrero-Muñoz MJ, Castillo-Carranza DL (2017) Tau oligomers: cytotoxicity, propagation, and mitochondrial damage. *Front Aging Neurosci* 9
116. Simrén J, Brum WS, Ashton NJ, Benedet AL, Karikari TK, Kvartsberg H, Sjoms E, Lussier FZ, Chamoun M, Stevenson J, Hopewell R, Pallen V, Ye K, Pascoal TA, Zetterberg H, Rosa-Neto P, Blennow K (2022) CSF tau368/total-tau ratio reflects cognitive performance and neocortical tau better compared to p-tau181 and p-tau217 in cognitively impaired individuals. *Alzheimers Res Ther* 14:192. <https://doi.org/10.1186/s13195-022-01142-0>

117. Sohal VS, Zhang F, Yizhar O, Deisseroth K (2009) Parvalbumin neurons and gamma rhythms enhance cortical circuit performance. *Nature* 459:698–702. <https://doi.org/10.1038/nature07991>
118. Sperling RA, Dickerson BC, Pihlajamaki M, Vannini P, LaViolette PS, Vitolo OV, Hedden T, Becker JA, Rentz DM, Selkoe DJ, Johnson KA (2010) Functional alterations in memory networks in early Alzheimer's disease. *Neuromolecular Med* 12:27–43. <https://doi.org/10.1007/s12017-009-8109-7>
119. Stam CJ, de Haan W, Daffertshofer A, Jones BF, Manshanden I, van Walsum AM, Montez T, Verbunt JPA, de Munck JC, van Dijk BW, Berendse HW, Scheltens P (2009) Graph theoretical analysis of magnetoencephalographic functional connectivity in Alzheimer's disease. *Brain J Neurol* 132:213–224. <https://doi.org/10.1093/brain/awn262>
120. Stan GF, Church TW, Randall E, Harvey JRM, Brown JT, Wilkinson KA, Hanley JG, Marrion NV (2022) Tau isoform-specific enhancement of L-type calcium current and augmentation of afterhyperpolarization in rat hippocampal neurons. *Sci Rep* 12:15231. <https://doi.org/10.1038/s41598-022-18648-0>
121. Stefanovski L, Triebkorn P, Spiegler A, Diaz-Cortes M-A, Solodkin A, Jirsa V, McIntosh AR, Ritter P (2019) Alzheimer's Disease Neuroimaging Initiative. Linking molecular pathways and large-scale computational modeling to assess candidate disease mechanisms and pharmacodynamics in Alzheimer's disease. *Front Comput Neurosci* 13:54. <https://doi.org/10.3389/fncom.2019.00054>
122. Targa Dias Anastacio H, Matosin N, Ooi L (2022) Neuronal hyperexcitability in Alzheimer's disease: what are the drivers behind this aberrant phenotype? *Transl Psychiatry* 12:1–14. <https://doi.org/10.1038/s41398-022-02024-7>
123. Teles-Grilo Ruivo LM, Mellor JR (2013) Cholinergic modulation of hippocampal network function. *Front Synaptic Neurosci* 5:2. <https://doi.org/10.3389/fnsyn.2013.00002>
124. Tracy TE, Gan L (2018) Tau-mediated synaptic and neuronal dysfunction in neurodegenerative disease. *Curr Opin Neurobiol* 51:134–138. <https://doi.org/10.1016/j.conb.2018.04.027>
125. Uhlenbeck GE, Ornstein LS (1930) On the theory of the brownian motion. *Phys Rev* 36:823–841. <https://doi.org/10.1103/PhysRev.36.823>
126. Vardalaki D, Chung K, Harnett MT (2022) Filopodia are a structural substrate for silent synapses in adult neocortex. *Nature* 612:323–327. <https://doi.org/10.1038/s41586-022-05483-6>
127. Verret L, Mann EO, Hang GB, Barth AMI, Cobos I, Ho K, Devidze N, Masliah E, Kreitzer AC, Mody I, Mucke L, Palop JJ (2012) Inhibitory interneuron deficit links altered network activity and cognitive dysfunction in Alzheimer model. *Cell* 149:708–721. <https://doi.org/10.1016/j.cell.2012.02.046>
128. Vertes RP, Hoover WB, Viana Di Prisco G (2004) Theta rhythm of the hippocampus: subcortical control and functional significance. *Behav Cogn Neurosci Rev* 3:173–200. <https://doi.org/10.1177/1534582304273594>
129. Ward SM, Himmelstein DS, Lancia JK, Binder LI (2012) Tau oligomers and tau toxicity in neurodegenerative disease. *Biochem Soc Trans* 40:667–671. <https://doi.org/10.1042/BST20120134>
130. Williams JH, Kauer JA (1997) Properties of carbachol-induced oscillatory activity in rat hippocampus. *J Neurophysiol* 78:2631–2640. <https://doi.org/10.1152/jn.1997.78.5.2631>
131. Winson J (1978) Loss of hippocampal theta rhythm results in spatial memory deficit in the rat. *Science* 201:160–163. <https://doi.org/10.1126/science.663646>
132. Witton J, Staniaszek LE, Bartsch U, Randall AD, Jones MW, Brown JT (2016) Disrupted hippocampal sharp-wave ripple-associated spike dynamics in a transgenic mouse model of dementia. *J Physiol* 594:4615–4630. <https://doi.org/10.1113/jphysiol.2014.282889>
133. Wu X, Ji G-J, Geng Z, Wang L, Yan Y, Wu Y, Xiao G, Gao L, Wei Q, Zhou S, Wei L, Tian Y, Wang K (2022) Accelerated intermittent theta-burst stimulation broadly ameliorates symptoms and cognition in Alzheimer's disease: a randomized controlled trial. *Brain Stimulat* 15:35–45. <https://doi.org/10.1016/j.brs.2021.11.007>
134. Wu X, Ji G-J, Geng Z, Zhou S, Yan Y, Wei L, Qiu B, Tian Y, Wang K (2020) Strengthened theta-burst transcranial magnetic stimulation as an adjunctive treatment for Alzheimer's disease: an open-label pilot study. *Brain Stimulat* 13:484–486. <https://doi.org/10.1016/j.brs.2019.12.020>
135. Zhang J, Yang Y, Li H, Cao J, Xu L (2005) Amplitude/frequency of spontaneous mEPSC correlates to the degree of long-term depression in the CA1 region of the hippocampal slice. *Brain Res* 1050:110–117. <https://doi.org/10.1016/j.brainres.2005.05.032>
136. Zhang W, Falcon B, Murzin AG, Fan J, Crowther RA, Goedert M, Scheres SH (2019) Heparin-induced tau filaments are polymorphic and differ from those in Alzheimer's and Pick's diseases. *Elife* 8:e43584. <https://doi.org/10.7554/eLife.43584>
137. Zhu G, Liu Y, Wang Y, Bi X, Baudry M (2015) Different patterns of electrical activity lead to long-term potentiation by activating different intracellular pathways. *J Neurosci* 35:621–633. <https://doi.org/10.1523/JNEUROSCI.2193-14.2015>
138. Zott B, Simon MM, Hong W, Unger F, Chen-Engerer H-J, Frosch MP, Sakmann B, Walsh DM, Konnerth A (2019) A vicious cycle of β amyloid-dependent neuronal hyperactivation. *Science* 365:559–565. <https://doi.org/10.1126/science.aay0198>

Publisher's Note

Springer Nature remains neutral with regard to jurisdictional claims in published maps and institutional affiliations.

Ready to submit your research? Choose BMC and benefit from:

- fast, convenient online submission
- thorough peer review by experienced researchers in your field
- rapid publication on acceptance
- support for research data, including large and complex data types
- gold Open Access which fosters wider collaboration and increased citations
- maximum visibility for your research: over 100M website views per year

At BMC, research is always in progress.

Learn more biomedcentral.com/submissions

